Developing Advanced Techniques on Modeling and System Identification of Piezoelectric Energy Harvesting Systems

by

Seyedmorteza Hoseyni

A Dissertation Submitted to the

Graduate School of Sciences and Engineering

in Partial Fulfillment of the Requirements for

the Degree of

Doctor of Philosophy

in

Mechanical Engineering

KOÇ ÜNİVERSİTESİ

January 2024

Developing Advanced Techniques on Modeling and System Identification of Piezoelectric Energy Harvesting Systems

Koç University

Graduate School of Sciences and Engineering

This is to certify that I have examined this copy of a doctoral dissertation by

Seyedmorteza Hoseyni

and have found that it is complete and satisfactory in all respects, and that any and all revisions required by the final examining committee have been made.

Committee Members:

Prof. Ipek Basdogan

Prof. Cagatay Basdogan

Prof. Murat Sozer

Assoc. Prof. Bekir Bediz

Assist. Prof. Amirreza Aghakhani

Date: January 2024

Dedication here (Optional)

ABSTRACT

Developing Advanced Techniques on Modeling and System Identification of Piezoelectric Energy Harvesting Systems

Seyedmorteza Hoseyni

Doctor of Philosophy in Mechanical Engineering

January 2024

Ambient vibration is the most available and promising source of energy that can be converted into electrical energy through several techniques and be used for powering small electronic devices. The advantage of harvesting ambient vibration energy is the removal of external power sources like batteries with maintenance cost and chemical waste. Among the diverse methods for vibration-based energy harvesting, piezoelectric materials stand out for their impressive power density and adaptability in manufacturing across desired geometries and scales. Piezoelectric energy harvesters, also, enable the researchers to develop self-powered devices and systems, such as structural health monitoring of 2D components in marine, aerospace, and automotive structures. Vibration-based piezoelectric energy harvesting consists of a piezoelectric transducer structurally coupled with a vibrating host structure which provides kinetic energy to be converted into electrical energy. A harvesting circuit is also connected electrically to the piezoelectric for regulating the harvested electrical energy.

The vibrating host structure has been extensively studied for beams with variable cross sections and several shapes. Plate structures, as an alternative to beams, are more suitable for piezoelectric energy harvesting not only because of their availability in practical applications

but also because of capability of providing broadband energy harvesting. On the other hand, advanced electrical circuits have been introduced to provide stable electrical power flow i.e., DC power output, and improve the efficiency of the energy harvesting system. However, the research in the mechanical part overlooked the use of advanced harvesting circuits and also the studies in the electrical part is limited to simple vibrating structures considering only one vibration mode of structure as an equivalent mass-stiffness-damper system. Therefore, this thesis is dedicated to bridge the research gap between the electrical advancements and mechanical studies on piezoelectric energy harvesting.

The first part of this work focuses on developing an analytical model for multi-modal piezoelectric energy harvesting on a thin plate structure integrated with an advanced harvesting circuit i.e., synchronized switch harvesting on inductor (SSHI). The analytical solution is developed based on an equivalent impedance approach to predict the steady-state electrical response of the harvester as a closed-form solution. The experiments are conducted to validate the analytical solution for the system's first and second vibration modes. The energy harvesting performance of the SSHI circuit is compared against the standard rectifier, showing 183% and 134% power output enhancement for the first and second vibration modes, respectively. Additionally, the experimental results reveal that integration of SSHI to a plate-like harvester introduces a multi-switching behavior rather than a standard single-switching behavior due to the multimodal vibrational characteristics of the plate.

Equivalent circuit modeling (ECM) is a useful tool for piezoelectric energy harvesters to analyze the electromechanical response of the system especially when complex host structure geometries and nonlinear circuits are used in the harvesting systems. At the second part of the thesis, we present an experimental admittance-based system identification method that allows us to identify the multi-modal ECM without prior knowledge of the host plate's geometry and/or physical properties of the piezoelectric patches. Using the proposed experimental method, we obtain the electromechanical frequency-response admittance of the PEH system at each vibration mode, and thereby, we calculate the equivalent system parameters. Additionally, a novel experimental technique is presented for the identification of the equivalent voltage sources associated with each LCR branch of the ECM. The derived ECM is experimentally validated for single and multiple piezoelectric patch harvesters on a plate. The electrical frequency response of the system has been validated for standard AC and rectifier circuits using SPICE software. Overall, the proposed admittance-based system identification is an accurate and robust method to identify the equivalent system parameters, making it a practical and reliable tool for modeling piezoelectric energy harvesting systems.

ÖZETÇE

Piezoelektrik Enerji Toplama Sisteminin Modelleme ve Sistem Tanımlama Konusunda Gelişmiş Teknikler Geliştirme.

Seyedmorteza Hoseyni

Makine Muhendisligi, Doktora

Ocak 2024

Çevre titreşimi, birkaç teknik aracılığıyla elektrik enerjisine dönüştürülebilen ve küçük elektronik cihazları beslemek için kullanılabilen en yaygın ve umut verici enerji kaynağıdır. Ambiyans titreşimi enerjisi toplamanın avantajı, bakım maliyeti ve kimyasal atık gibi harici güç kaynaklarının, örneğin pillerin ortadan kaldırılmasıdır. Titreşim tabanlı enerji toplama için çeşitli yöntemler arasında, istenen geometriler ve ölçeklerde üretimde etkileyici güç yoğunluğu ve uyarlanabilirlikleri nedeniyle piezoelektrik malzemeler öne çıkar. Piezoelektrik enerji toplayıcıları, ayrıca deniz, havacılık ve otomotiv yapılarında 2B bileşenlerin yapısal sağlık izlemesi gibi kendi kendini besleyen cihazlar ve sistemler geliştirmek için araştırmacılara olanak tanır. Titreşim tabanlı piezoelektrik enerji toplama, kinetik enerji sağlayan titreşen bir ana yapı ile yapısal olarak bağlantılı bir piezoelektrik transdüserden oluşur ve bu enerjinin elektrik enerjisine dönüştürülmesini sağlar. Toplanan elektrik enerjisini düzenlemek için bir toplama devresi elektriksel olarak piezoelektrikle bağlanmıştır.

Titreşen ana yapının değişken kesitli kirişler ve birkaç şekil için yoğun bir şekilde incelendiği görülmüştür. Kirişlere alternatif olarak, piezoelektrik enerji toplama için plaka yapıları hem

pratik uygulamalarda bulunabilirlikleri hem de geniş bant enerji toplama sağlama yetenekleri nedeniyle daha uygun görünmektedir. Öte yandan, stabil elektrik güç akışı, yani DC güç çıkışı sağlamak ve enerji toplama sisteminin verimliliğini artırmak için gelişmiş elektrik devreleri tanıtılmıştır. Ancak, mekanik kısımdaki araştırma, gelişmiş toplama devrelerinin kullanımını göz ardı etmiş ve elektrik kısmındaki çalışmalar, sadece bir titreşim modunu dikkate alan basit titreşen yapıları içermiştir.

Bu tez, piezoelektrik enerji toplama üzerine elektriksel ilerlemeler ile mekanik çalışmalar arasındaki araştırma boşluğunu kapatmaya adanmıştır. Bu çalışmanın ilk kısmı, ince bir plaka yapısına entegre edilmiş gelişmiş bir toplama devresi olan, endüktrde senkronize anahtarlamalı toplama (SSHI) ile çoklu modlu piezoelektrik enerji toplama için analitik bir model geliştirmeye odaklanmaktadır. Analitik çözüm, harvester'ın sürekli durum elektriksel yanıtını kapalı bir form çözümü olarak tahmin etmek için bir eşdeğer empadans yaklaşımına dayanarak geliştirilmiştir. Deneyler, sistem için ilk ve ikinci titreşim modlarının analitik çözümünü doğrulamak için yapılmıştır. SSHI devresinin enerji toplama performansı, standart doğrultucuyla karşılaştırılmış ve sırasıyla birinci ve ikinci titreşim modları için %183 ve %134 güç çıkışı artışı göstermiştir. Ayrıca, deneysel sonuçlar, plaka benzeri bir harvester'a SSHI entegrasyonunun, plakanın çoklu modal titreşim özellikleri nedeniyle standart tek anahtarlamalı bir davranış yerine çoklu anahtarlamalı bir davranış tanıttığını ortaya koymaktadır.

Eşdeğer devre modelleme (EDM), karmaşık ana yapı geometrileri ve doğrusal olmayan devrelerin enerji toplama sistemlerinde kullanılması durumunda, piezoelektrik enerji toplayıcıları için elektromekanik yanıtı analiz etmek için kullanışlı bir araçtır. Tezin ikinci bölümünde, piezoelektrik yamaçların fiziksel özelliklerine ve/veya ana plakanın geometrisine önceden bilgi sahibi olmadan çoklu modal EDM'nin tanımlanmasına izin veren deneysel bir admans tabanlı sistem tanımlama yöntemi sunuyoruz. Önerilen deneysel yöntem kullanılarak, her titreşim modunda PEH sisteminin elektromekanik frekans tepki admansını elde ediyoruz ve böylece eşdeğer sistem parametrelerini hesaplıyoruz. Ayrıca, EDM'nin her LCR dalıyla ilişkilendirilen eşdeğer voltaj kaynaklarının tanımlanması için yeni bir deneysel teknik sunulmaktadır. Elde edilen EDM, bir plakadaki tekli ve çoklu piezoelektrik yamaç toplayıcıları için deneysel olarak doğrulanmıştır. Sistemin elektrik frekans tepkisi, SPICE yazılımı kullanılarak standart AC ve doğrultucu devreleri için doğrulanmıştır. Genel olarak, önerilen admans tabanlı sistem tanımlaması, eşdeğer sistem parametrelerini tanımlamak için doğru ve sağlam bir yöntem olup, piezoelektrik enerji toplama sistemlerini modellemek için pratik ve güvenilir bir araç haline getirir.

ACKNOWLEDGMENTS

I extend my heartfelt appreciation to my supervisor, **Prof. Ipek Basdogan**, whose unwavering support and guidance have been invaluable throughout my studies. Their collective encouragement and expertise have played an instrumental role in shaping my academic and professional growth, for which I am truly grateful.

I am also indebted to **Prof. Amirreza Aghakhani** for his role as a phenomenal mentor, offering me invaluable insights and wisdom.

I express my sincere thanks to **Prof. Elie Lefeuvre** for his collaborative efforts, which have enriched my research experience and broadened my perspectives.

I am immensely grateful to the **Graduate School of Science and Engineering** (GSSE) for awarding me the scholarship that has significantly eased my academic journey.

TABLE OF CONTENTS

LIST OF TABLES

LIST OF FIGURES

CHAPTER 1

INTRODUCTION

1.1 Multimodal piezoelectric energy harvesting

Piezoelectric energy harvesting is a growing area of research due to its potential to provide a clean and sustainable source of energy by converting mechanical energy, such as vibrations, into electrical energy that can be stored and utilized for various applications [Sharma et al., 2022]. Researchers are investigating piezoelectric energy harvesting for several reasons. One of the main reasons is to develop self-powered devices and systems, such as wearable devices and IoT (Internet of Things) sensors, that do not require a separate power source [Sezer & Koç, 2021]. This can reduce the reliance on batteries, which can be expensive and have a limited lifespan, and increase the efficiency of energy conversion so that more energy can be obtained from a given amount of mechanical energy [Sezer & Koç, 2021; Sharma et al., 2022]. Another reason is to provide a source of energy in remote or inaccessible locations where traditional power sources are not available. This can have significant implications for various industries, such as transportation, and healthcare, that require energy in these types of environments [Sezer & Koç, 2021]. Furthermore, researchers are exploring the use of complex structured materials such as polymers and ceramics to improve the performance of piezoelectric energy harvesting systems [Li & Lee, 2022]. By using advanced materials and optimizing the energy conversion process, the efficiency and effectiveness of piezoelectric energy harvesting systems can be increased [Wu et al., 2021].

Piezoelectric energy harvesters are structurally integrated with a host structure which provides the kinetic energy to be converted into electrical energy. The geometry of the host structure for piezoelectric energy harvesters have taken various forms in the literature [Ahmad et al., 2016; Aridogan et al., 2013; Xie et al., 2020], where the cantilevered beams has been extensively investigated by researchers due to their relative simplicity of implementation [Cottone et al., 2012; Erturk & Inman, 2008a; Erturk & Inman, 2009; Zheng et al., 2015]. The cantilevered beam with variable cross section [Ben Ayed et al., 2013; Dietl & Garcia, 2010; Raju et al., 2017; Salmani & Rahimi, 2018; Syed et al., 2018; Xie et al., 2017; Yang et al., 2017; Zhou et al., 2016], arc-shaped beams [Jung et al., 2015; Jung et al., 2016; Leinonen et al., 2013; Wang et al., 2020; Zhou et al., 2021], M-shaped beams [Chen et al., 2021; Leadenham & Erturk, 2015], and L-shaped beams [Huang et al., 2020; Tian et al., 2020], star-shaped metamaterial [Wang et al., 2022] were considered to optimize the response of the system. However, the cantilever beam harvesters are strongly dependent on the narrow excitation frequency range, where the optimal performance typically happens at the primary resonance frequency. Consequently, if the vibration of ambient energy sources does not match the resonance frequency of the beam, the performance of the harvester drops drastically. Therefore, the application of cantilever beam harvesters is limited to controlled scenarios with specific excitation frequency. However, in practical applications, the vibration frequency spectrum of the environment is random and fluctuating [Tang et al., 2010]. Moreover, the cantilever beams have limited bandwidth characteristics for energy harvesting purposes, since the consecutive resonance frequencies are far from each other, hence broadband energy harvesting cannot be performed [Erturk et al., 2009].

Recently, plate-like structures have drawn researchers' attention not only because of their availability in practical applications such as marine, aerospace, and automotive structures but also because of their capability of providing broadband energy harvesting systems due to their close consecutive resonance frequencies. [U Aridogan et al., 2014] presented an analytical solution and experimental validation for the plate-like piezo-patch energy harvesters with a resistive load as an external circuit which provides AC power output. The same research group pursued their research for a general case as multiple piezo-patch harvesters on a plate where the patches connected in parallel and series configurations satisfying the broadband energy harvesting through multiple vibration modes [Ugur Aridogan et al., 2014]. Improvement of estimation of the power output has been achieved considering the inertial and stiffness components of piezo-patches using Rayleigh-Ritz method [Yoon et al., 2016].

The majority of investigations in the electrical part of piezoelectric energy harvesting systems are dedicated to developing advanced harvesting circuits which provide more effective and efficient energy conversion. Energy harvesting interfaces are essential components in piezoelectric energy harvesting systems, as they serve to convert the mechanical energy applied to the piezoelectric material into a usable electrical energy [Lefeuvre et al., 2006; Liao & Liang, 2019]. One of the simplest forms of energy harvesting interfaces is the resistive load, which converts the piezoelectric voltage into a usable electrical current [Erturk, 2012; Guyomar et al., 2005b]. In practice, stable power flow is required for electronic devices, hence DC output is more desirable and can be captured by using an AC to DC convertor circuit which has a nonlinear behavior [Y. Shu & I. Lien, 2006]. The harvesting circuits including AC to DC convertor has been extensively studied where most investigations focused on the beam as the host structure [Liang & Liao, 2008; Ottman et al., 2002; Y. Shu & I. Lien, 2006]. Improvements on DC power output of the PEH can be achieved by adding a series connected switch and inductor to the rectifier. This technique is called Synchronized Switch Harvesting on Inductor (SSHI) [Claude Richard, 2007; Guyomar et al., 2005b; Lallart et al., 2008; Lefeuvre et al., 2006; Liang & Liao, 2012b]. During the vibration, the polarity of the piezo patch is inversed by triggering the switch only at the peak displacements of PEH. This artificial manipulation enhances the voltage generated by the piezoelectric element [Guyomar et al., 2005b; Y. Shu et al., 2007]. Previous studies have presented an analytical solution for the SSHI circuit, which can estimate the power output of the harvester only at its resonance frequency [Guyomar et al., 2005a; Lefeuvre et al., 2006]. Furthermore, The difference in phase between the excitation and the mass velocity has also been taken into account in an improved analytical solution. [I. Lien et al., 2010; Y. Shu et al., 2007]. The equivalent impedance approach has been proposed to obtain a closed form solution for rectifier, Parallel-SSHI, and Series-SSHI interfaces integrated with an array of piezoelectric energy harvesters connected in parallel [Lien & Shu, 2012] and in series [Lin et al., 2013] configuration. This approach is an approximation method and is based on simplifying the model to the fundamental harmonics of the system [Junrui & Wei-Hsin, 2010; Liang & Liao, 2012a]. New topologies of the self-powered SSHI circuit have been proposed to modify the peak detection units [Liang & Liao, 2012b] and reduce the power loss of the circuit [Eltamaly & Addoweesh, 2017].

It has been proved that the harvesting circuit has a reaction to the dynamic of the host structure [J. Liang & W.-H. Liao, 2011]. In practice, the more extracted power, the more induced damping effect [Liang & Liao, 2008]. However, most of the studies regarding the effect of the harvesting circuits on the dynamic of the structure are only focused on the cantilevered beams. Development of the models are carried out considering equivalent mass + springer + damper + piezo structure of the system around fundamental resonance frequency [Erturk & Inman, 2008b; Lefeuvre et al., 2006; J. R. Liang & W. H. Liao, 2011; Liao & Liang, 2019; Y. Shu et al., 2007]. Despite all the advantages of plate-like structures for energy harvesting purposes i.e., availability in practical applications such as marine, aerospace, and automotive structures, and capability of providing broadband energy harvesting, the investigations on thin plate are limited to the simple harvesting circuits [Aridogan et al., 2013; U Aridogan et al., 2014; Ugur Aridogan et al., 2014; Yoon et al., 2016]. A multi-mode equivalent circuit modeling of PEH integrated with standard harvesting circuit has been developed [Bayik et al., 2016]. Moreover, analytical solution of wideband energy harvesting with multiple patches on a plate using a rectifier has been developed based on equivalent impedance approach [Aghakhani & Basdogan, 2017]. A distributed-parameter model of a thin plate with multiple piezo-patches was developed based on standard modal analysis method. Piezoelectric metamaterial plate with local resonators integrated with synchronized charge extraction circuit was investigated to improve the performance of the harvesting system [Chen et al., 2020]. Despite all the studies on the piezoelectric energy harvesting systems, the integration of self-powered SSHI circuit with piezoelectric energy harvester structurally coupled with a plate-like host structure is missing in the literature. Therefor, the motivation of Chapter 2 is to study the energy harvesting performance of the self-powered SSHI circuit integrated with piezoelectric on a more available structure in practical applications i.e., plate with dense modal properties, and to compare the power extraction capability of the SSHI interface with the standard harvesting circuit. This system can be used in powering small electronic devices and structural health monitoring of 2D components in marine, aerospace, and automotive structures, as well as buildings.

1.2 Equivalent Circuit Modeling of Piezoelectric Energy Harvesters

Several methods have been proposed to evaluate the performance of energy harvesting systems. Analytical solutions have been developed to predict the mechanical and electrical response of piezoelectric energy harvesters on cantilevered beams [Erturk, 2012; Erturk & Inman, 2008a], curved beams [Wang et al., 2020], M-shaped beams [Leadenham & Erturk, 2015], and thin plates [U Aridogan et al., 2014; Ugur Aridogan et al., 2014] where the harvesting circuit has been considered as a resistive load. Moreover, analytical solutions have been developed for cantilevered beams integrated with advanced harvesting circuits [I. C. Lien et al., 2010; Y. C. Shu & I. C. Lien, 2006; Y. C. Shu et al., 2007]. An equivalent impedance approach based on simplifying the system to fundamental harmonics of the circuit has been proposed to predict the electrical response of an array of piezoelectric beams integrated with nonlinear harvesting circuits [Lien & Shu, 2012; Lin et al., 2013]. This method was extended for thin plates integrated with a standard rectifier [Aghakhani & Basdogan, 2017] and parallel SSHI circuit [Hoseyni et al., 2023]. The finite element method is capable of simulating harvesting structures with complex geometries, where M-shaped beams [Chen et al., 2021], L-shaped beams [Huang et al., 2020], and thin plates [Aridogan et al., 2013] have been simulated with resistive loads as harvesting circuits. A finite element method has been proposed to evaluate piezoelectric energy harvesters of complex geometry with a standard AC-DC rectified circuit [Qian et al., 2021]. Piezoelectric energy harvesters can also be approximated with their equivalent circuit model (ECM) [Lan et al., 2022; Zhang et al., 2021]. A circuit simulator software i.e., LTSpice can be used to investigate the performance of the harvester using ECM with any circuit elements. In previous studies, the ECM of piezoelectric energy harvesters on a cantilevered beam [Elvin & Elvin, 2008] and thin plate [Aghakhani & Basdogan, 2018] have been extracted from the analytical model. On the other hand, as an alternative method, the ECM of the harvesting system can be also determined based on the admittance of the piezoelectric element using the finite element method [Yang & Tang, 2009]. The performance of a piezoelectric energy harvester integrated with advanced circuits has been evaluated for a cantilever beam [Seok et al., 2022] and a thin plate [Bayik et al., 2016] considering the ECM obtained from finite element analysis.

Equivalent circuit modeling is a valuable approach for integrating the piezoelectric harvester with advanced harvesting circuits. However, the proposed methods of determining the parameters of piezoelectric energy harvester are based on analytical and/or finite element analysis. Analytical models are applicable to the harvesting system with simple structural geometry, and they are based on theories that simplify the structure to some extent e.g., Euler-Bernoulli beam theory, and Kirchhoff plate theory. Besides, the analytical approaches presented for advanced circuits approximate the electrical behavior only at the fundamental frequency [I. C. Lien et al., 2010; Y. C. Shu & I. C. Lien, 2006; Y. C. Shu et al., 2007]. Finite element analysis has the capability of simulating energy harvesters with complex geometries however the available commercial software only allows for simple resistive loads as the electrical elements and lacks the capability of integrating nonlinear components of advanced circuits. Although analytical solutions and finite element simulations can predict the trend of harvesters' response, they cannot represent the actual behavior of the harvesting system due to simplifications and a lack of applying the exact values of mechanical, electrical, and modal properties of the system. Considering the drawbacks of analytical and finite element methods, a more promising approach should be developed to determine the parameters of ECM directly from the actual experimental setup. Therefore, a robust and accurate experimental method for identifying the multi-mode ECM directly from an experimental setup was proposed in Chapter 3. The method is based on the electromechanical admittance of the PEH which provides information for obtaining the parameters of the ECM.

CHAPTER 2
MULTIMODAL PIEZOELECTRIC ENERGY HARVESTING ON A THIN PLATE INTEGRATED WITH SSHI CIRCUIT.

2.1 Introduction

In this chapter, electromechanical equations of the piezoelectric energy harvester on a thin plate are integrated with the equivalent load impedance of self-powered SSHI circuit for the first time, to predict the behavior of the harvesting system. Unlike the previous study [Aghakhani & Basdogan, 2017], the effects of inertia and stiffness of piezoelectric are considered in this study. Due to discontinuities on the structure, Rayleigh-Ritz method is used to perform modal analysis and obtain natural frequencies and mode shapes of the structure. Besides, an experimental setup is developed to examine the harvesting performance of the SSHI circuit for the first and the second vibration modes of the host plate. Experimental results show that the SSHI circuit affects the dynamic of plate drastically in high resistive loads because of high modal density of thin plate. The effect of damping due to the SSHI interface is visible as ripples in the piezoelectric voltage waveforms. These ripples also change the switching behavior of the SSHI interface. An undesired multiple switching behavior of the SSHI circuit at high resistive load is observed which reduces the functionality of interface for energy harvesting purposes. It is shown that the analytical voltage outputs are in good agreement with the experimental results for the first and the second modes when there is just one switch in each half period of the vibration i.e., single switching. Besides, the experimental results show that the SSHI circuit does not switch at low piezoelectric voltage levels which means it is not active and behaves as a standard rectifier. A detailed study is carried out to show all these switching behaviors of the SSHI circuit along with the voltage and power output characteristics. Furthermore, it is demonstrated that the SSHI circuit improves the maximum DC output power of the harvester compared to a standard AC input-DC output (i.e., a standard rectifier) in both modes.

2.2 Analytical model

The analytical model of the electromechanical system consists of a thin plate with clamped boundary conditions for all four edges (CCCC) which is structurally integrated with a piezoelectric patch of thickness (h_p) connected to an SSHI interface (Figure 2.1).

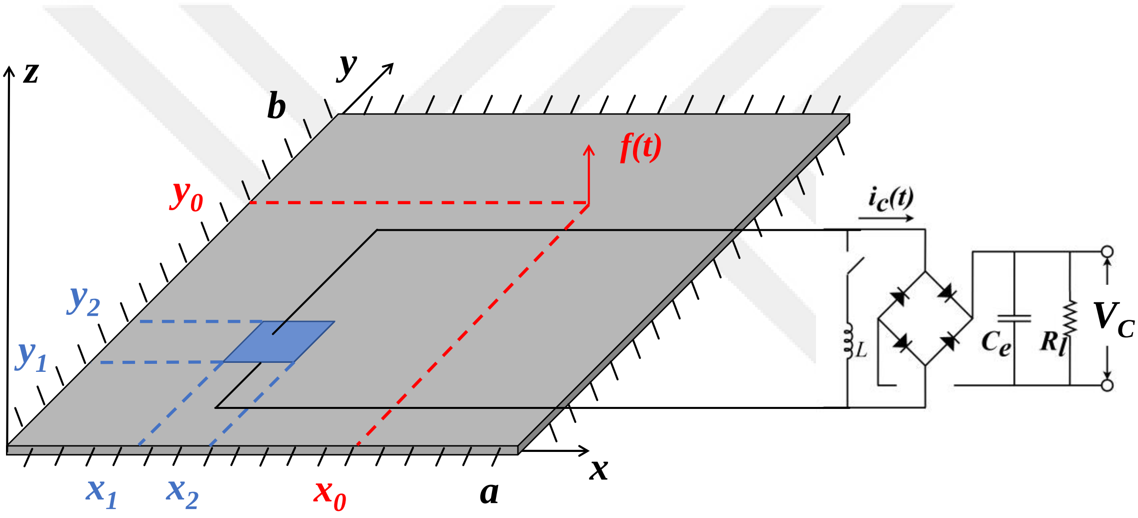

Figure 2.1: Schematic of the piezoelectric energy harvester attached to a thin plate.

The piezoelectric patch is assumed to be perfectly bonded to the host structure. The model is based on Kirchhoff plate theory since the thickness of plate (h_s) is assumed to be much smaller than the length (a) and width (b). Consequently, the piezoelectric energy harvester (PEH) is in a plane stress state, and the effect of transverse shear deformation can be neglected. It is assumed that the material of the host structure is isotropic. The material of the piezoelectric is transversely isotropic, and the direction of generated voltage is perpendicular to the applied strain. The model is developed for a transverse point force $f(t)$ which excites the plate at the position coordinates (x_0, y_0). The subscripts s and p stand for the parameters related to the host structure and piezoelectric patch. The Hamilton principle is used to derive the equation of motion which includes the effect of inertia and stiffness of the piezoelectric patch. The electromechanical equations of motion of PEH were previously developed by [Yoon et al., 2016]. Due to the discontinuity of the geometry at the piezoelectric edges, the Rayleigh-Ritz method is implemented to conduct modal analysis and approximate the undamped natural frequencies and mode shapes of the model. The Rayleigh-Ritz method is based on discretizing the distributed-parameter model to obtain an approximation of the modal parameters. Linear combination of modes based on modal expansion theorem is considered to obtain an approximation of the displacement of PEH.

$$w(x,y,t) = \sum_{m=1}^{N}\sum_{n=1}^{N} \varphi_{mn}(x,y).\eta_{mn}(t) \tag{2.1}$$

where $\varphi_{mn}(x,y)$ is the mode shape and $\eta_{mn}(t)$ is the time dependent modal coordinate of the plate, for the mnth vibration mode *(m, n = 1, 2, ..., N)*. N is a degree of approximation, and the convergence of natural frequencies happens when N is large enough. A set of N^2 electromechanical equations of motion can be written for PEH corresponding to N^2 degrees-of-freedom. Based on the orthogonality of modes, a set of N^2 independent equations of motion can be obtained by modal coordinate transformation. Differential equation of motion for a plate integrated with a piezo-patch in modal coordinate is [Yoon et al., 2016]

$$\frac{d^2\eta_{mn}(t)}{dt^2} + 2\zeta_{mn}\omega_{mn}\frac{d\eta_{mn}(t)}{dt} + \omega_{mn}^2\eta_{mn}(t) - \Theta_{mn}v_p(t) = f_{mn}(t) \tag{2.2}$$

where $v_p(t)$ is the piezoelectric voltage, ω_{mn} is the undamped natural frequency and ζ_{mn} is the modal damping ratio for the mnth vibration mode. Θ_{mn} corresponds to the modal electromechanical coupling of the piezoelectric patch for mnth vibration mode and is defined as [Yoon et al., 2016]:

$$\Theta_{mn} = -\bar{e}_{31}\left(\frac{h_p + h_s}{2} - z_0\right)\int_{y1}^{y2}\int_{x1}^{x2}\left[\frac{\partial^2\varphi_{mn}(x,y)}{\partial x^2} + \frac{\partial^2\varphi_{mn}(x,y)}{\partial y^2}\right]dxdy \tag{2.3}$$

where $\bar{e}_{31}$ is piezoelectric constant, and $\varphi_{mn}(x,y)$ is the mass normalized eigenfunction of the plate for mnth vibration mode. z_0 is the location of the neutral surface in the areas in which the piezoelectric patch is attached. Modal forcing input which corresponds to the force for each mode shape is denoted by $f_{mn}(t)$ and is given by [Aghakhani & Basdogan, 2017]

$$f_{mn}(t) = f(t)\varphi_{mn}(x_0,y_0) \tag{2.4}$$

Equivalent circuit of a piezoelectric device can be presented as its internal electrode capacitance C_p in parallel with a set of parallel branches of second order LCR circuit which is equivalent to a velocity proportional current source (Figure 2.2) where $C_p = \bar{\varepsilon}_{33}^{S} \frac{l_p * w_p}{h_p}$ and $\bar{\varepsilon}_{33}^{S}$, l_p, w_p and h_p are the permittivity at constant strain, length, width, and thickness of piezoelectric patch, respectively [Yoon et al., 2016].

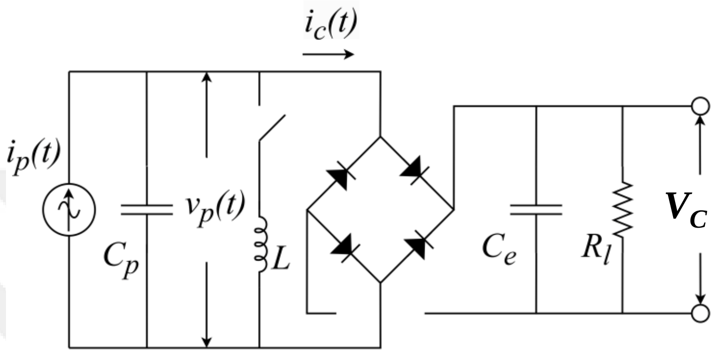

Figure 2.2: Equivalent circuit of a piezoelectric device.

The coupled circuit equation of piezoelectric is

$$C_p \frac{dv_p(t)}{dt} + i_c(t) = i_p(t)\,. \tag{2.5}$$

where $i_p(t)$ and $i_c(t)$ are the equivalent current source, and the current flowing into the SSHI circuit, respectively. It is worth noting that all the AC to DC circuits affect the behavior of the harvesting system. However, it can be assumed that the impact of the higher order harmonics due to the self-powered SSHI circuit is negligible compared to the fundamental component. Consequently, the model can be simplified where the equivalent current source $i_p(t)$ can be assumed to be perfectly harmonic, and piezoelectric voltage $v_p(t)$ can be regarded as its fundamental harmonic [Liang & Liao, 2012a]. The electrical equation in modal coordinates can be presented as [Yoon et al., 2016]

$$-\sum_{m=1}^{N}\sum_{n=1}^{N} \Theta_{mn} \frac{d\eta_{mn}(t)}{dt} + i_c(t) + C_p \frac{dv_p(t)}{dt} = 0 \tag{2.6}$$

Equivalent current source of piezoelectric harvester can be obtained from equations (2.5) and (2.6), as follows.

$$i_p(t) = \sum_{m=1}^{N} \sum_{n=1}^{N} \Theta_{mn} \frac{d\eta_{mn}(t)}{dt} \tag{2.7}$$

2.3 Equivalent impedance approach

SSHI harvesting interface refers to an inductance L connected in series with a switch which is in parallel with a rectifier bridge and piezoelectric patch as shown in Figure 2.2. The switch is always open except in time instant of extremum displacement. When the switch is triggered, the inductance L and capacitance of piezoelectric C_p form an oscillator circuit which reverses the voltage of the piezoelectric element. The inversion process consists of an energy loss in the inductor and the switch, therefore, an inversion quality factor Q_I can be defined for the SSHI circuit. Solving the electromechanical equations for the SSHI circuit integrated with a piezoelectric patch on a plate structure is not straight forward since the circuit consists of electrical components such as diodes and switches. Therefore, an equivalent impedance approach is used to solve the electromechanical equations.

Considering a transverse point force of $f(t) = F_0 e^{i\omega t}$ as harmonic input at frequency ω, and approximate the piezoelectric voltage with its fundamental harmonic $\left(v_p(t) = V_p e^{i\omega t}\right)$, the steady-state response of the system based on linear system assumption can be expressed as

$$\eta_{mn}(t) = \mathrm{H}_{mn} e^{i\omega t} \tag{2.8}$$

where H_{mn} and V_p are complex numbers. Inserting $f(t)$, equation (2.4), and equation (2.8) into equation (2.2), the complex modal response H_{mn} can be expressed as

$$H_{mn} = \frac{F_0 \varphi_{mn}(x_0, y_0) + V_p \Theta_{mn}}{\omega_{mn}^2 - \omega^2 + i2\zeta_{mn}\omega_{mn}\omega} \tag{2.9}$$

Inserting (2.8) into (2.7), steady-state form of velocity proportional current source of piezoelectric can be expressed as $i_p(t) = I_p e^{i\omega t}$ where the complex amplitude is

$$I_p = \sum_{m=1}^{N} \sum_{n=1}^{N} I_{mn} = \sum_{m=1}^{N} \sum_{n=1}^{N} [i\omega \Theta_{mn} H_{mn}] \tag{2.10}$$

The relation between the magnitude of the equivalent piezoelectric current source and the average output voltage can be calculated by [Lien & Shu, 2012]

$$V_c = \frac{2R_l}{\pi + (1 - q_I)C_p\omega R_l} I_p \tag{2.11}$$

Where q_I is the ratio of the piezoelectric voltage after switching and before switching $\left(q_I = \frac{V_p^{after}}{V_p^{before}} = e^{-\frac{\pi}{2Q_I}}\right)$ and Q_I is the inversion quality factor of the SSHI circuit. To obtain output voltage, let Z_{eq} be the equivalent impedance of the SSHI circuit plus piezoelectric capacitance as shown in Figure 2.3.

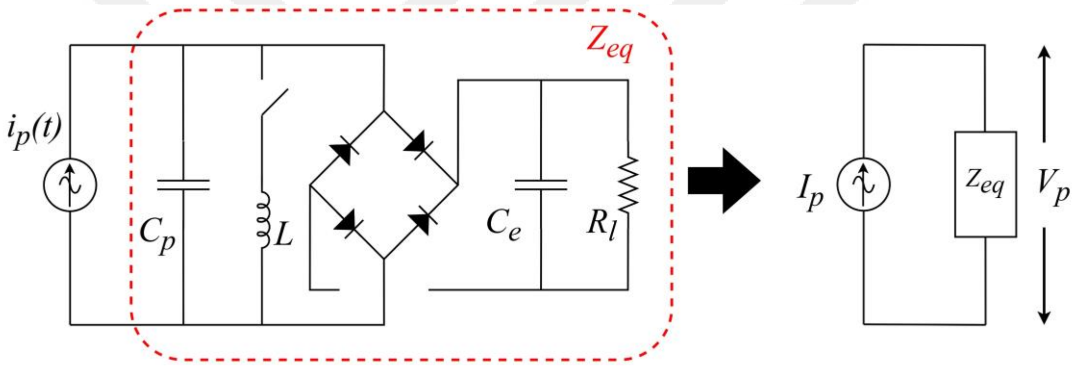

Figure 2.3: Equivalent impedance of a piezoelectric energy harvester integrated with SSHI interface.

For array of SDOF harvesters connected in parallel to the SSHI circuit, equivalent impedance model has been proposed as a function of resistive load R_l, capacitance of piezoelectric C_p, and excitation frequency ω [Lien & Shu, 2012]. Equivalent impedance is a complex value $(Z_{eq} = Z_R^{SSHI} + jZ_I^{SSHI})$ which is expressed as

$$Z_R^{SSHI} = \frac{2R_l\left[1 + \frac{(1 - q_I^2)}{2\pi}C_p\omega R_l\right]}{\left(\frac{\pi}{2} + \frac{(1 - q_I)}{2}C_p\omega R_l\right)^2}, \quad Z_I^{SSHI} = \frac{-\frac{(1 - q_I)}{2}R_l}{\left(\frac{\pi}{2} + \frac{(1 - q_I)}{2}C_p\omega R_l\right)} \tag{2.12}$$

The relation between the current flowing into Z_{eq} and the voltage across it can be expressed as

$$V_p = Z_{eq} I_p = Z_{eq} \sum_{m=1}^{N} \sum_{n=1}^{N} I_{mn} \tag{2.13}$$

Substituting $v_p(t)$, equations (2.8), and equations (2.13) into (2.2) and dividing both sides by the Θ_{mn}, the mechanical equation of piezoelectric harvester can be obtained as

$$(\omega_{mn}^2 - \omega^2 + i2\zeta_{mn}\omega_{mn}\omega)\frac{H_{mn}}{\Theta_{mn}} - Z_{eq} I_p = F_0 \frac{\varphi_{mn}(x_0, y_0)}{\Theta_{mn}} \tag{2.14}$$

Inserting equation (2.10) as the steady-state form of velocity proportional current source into equation (2.14), it can be showed that the equation can be expressed by the matrix equation as [Aghakhani & Basdogan, 2018]

$$\widehat{\boldsymbol{V}} = \widehat{\boldsymbol{Z}}\,\widehat{\boldsymbol{I}} \tag{2.15}$$

where $\widehat{\boldsymbol{V}}$ is a vector of dimension mn×1 and can be calculated as

$$\widehat{\boldsymbol{V}} = \left(\widehat{V}_{kl}\right) = -F_0 \frac{\varphi_{kl}(x_0, y_0)}{\Theta_{kl}}\ ,\ k = 1, 2, \dots, m;\ \ l = 1, 2, \dots, n. \tag{2.16}$$

and $\widehat{\boldsymbol{Z}}$ as a square matrix of dimension mn×mn is given by $\widehat{\boldsymbol{Z}} = Z_{eq}\boldsymbol{A} + diag(\boldsymbol{Z})$. Matrix $\boldsymbol{A}$ is of dimension $mn \times mn$ with all elements equal to one, and $diag(\boldsymbol{Z})$ is a diagonal matrix, where its diagonal elements are $\boldsymbol{Z} = [Z_{11}\ Z_{21} \dots\ Z_{mn}]^T$ and is obtained by:

$$Z_{kl} = \frac{2\zeta_{kl}\omega_{mn}}{(\Theta_{kl})^2} + i\,\frac{\omega^2 - \omega_{kl}^2}{\omega(\Theta_{kl})^2}\ ,\ k = 1, 2, \dots, m;\ \ l = 1, 2, \dots, n. \tag{2.17}$$

Solving equation (2.15) for the unknown $\widehat{\boldsymbol{I}}$ which includes I_{mn} as magnitude of equivalent current for each oscillating mode and inserting it into (2.11), the output voltage of the SSHI circuit can be extracted. Consequently, the DC power output of the harvester can be estimated by

$$P_c = \frac{{V_c}^2}{R_l} \tag{2.18}$$

Moreover, the complex modal response H_{mn} can be determined by equation (2.14). Thus, the mechanical modal coordinate $\eta_{mn}(t)$ is obtained, and transverse displacement of the plate at any point of (x, y) as a function of time can be obtained by:

$$w(x,y,t) = \sum_{m=1}^{N}\sum_{n=1}^{N} \varphi_{mn}(x,y).\eta_{mn}(t)$$
$$= \sum_{m=1}^{N}\sum_{n=1}^{N}\left\{\frac{\varphi_{mn}(x,y)}{\omega_{mn}^2 - \omega^2 + i2\zeta_{mn}\omega_{mn}\omega}.\left(F_0\varphi_{mn}(x_0,y_0)\right.\right.$$
$$\left.\left. + \Theta_{mn}Z_{eq}\sum_{m=1}^{N}\sum_{n=1}^{N} I_{mn}\right)\right\}.e^{i\omega t} \quad (2.19)$$

2.4 Model validation

2.4.1 Experimental setup

Experimental setup consists of a fully clamped (CCCC) aluminum plate which has been excited by a linear sine point force located at 0.087 and 0.087 m away from the bottom right corner of the plate in x and y directions, respectively. The piezo-patch harvesters (T105-A4E-602 manufactured by Piezo Systems, Inc.) were bonded on the aluminum plate (Figure 2.4), where the piezo patch on the left side has been used as the harvester and two other patches have been short circuited to eliminate the backward piezoelectric effect.

Table 2.1 introduces the geometric, mechanical, and electro-elastic properties of the experimental setup. A force transducer (PCB 208C02) was installed at the tip of the shaker to measure the dynamic force which is the reference input of the system and was used to determine the voltage frequency response (FRF) of the harvester. A laser Doppler vibrometer (Polytec PDV 100) measured the transvers velocity output of the plate. A resistance box which provides a wide range of resistance from 1 Ω through 1 MΩ has been used to generate desired resistive load.

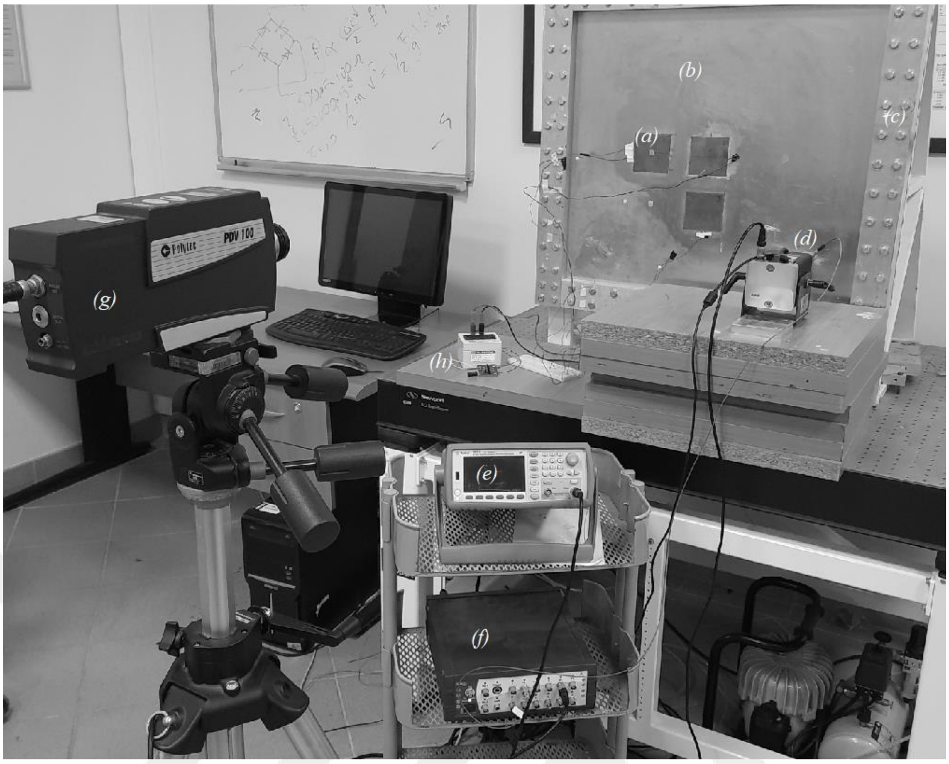

Figure 2.4: Experimental setup: (a) PZT; (b) aluminum plate; (c) clamping frame; (d) shaker and a force transducer; (e) signal generator; (f) data acquisition unit; (g) laser vibrometer; and (h) electrical circuit.

Table 2.1: Dimension and material properties of the plate and the piezo patch.

Property	Aluminium	Piezoceramic
Length (mm) X	580	72.4
Width (mm) Y	540	72.4
Thickness (mm)	1.9	0.267
Young’s modulus (GPa)	65.1	66
Mass density (Kg/m-3)	2575	7800
Piezoelectric constant (pm/V)	-	-190
Permittivity constant (nF/m)	-	10.38

The experiments were conducted considering three different harvesting circuits, i.e., resistive load, standard rectifier, and SSHI circuit (Figure 2.5). The aim of conducting the AC input-AC output experiment with resistive load was determination of modal damping ratios of the structure and initial validation of the model. On the other hand, a standard rectifier was used to assess the harvesting performance of the SSHI, since they both aim to extract DC power output. The SSHI circuit used in the experiment and the schematic of the circuit is available in Figure 2.6. The operation principle of this self-powered SSHI circuit was fully detailed in [Eltamaly & Addoweesh, 2017].

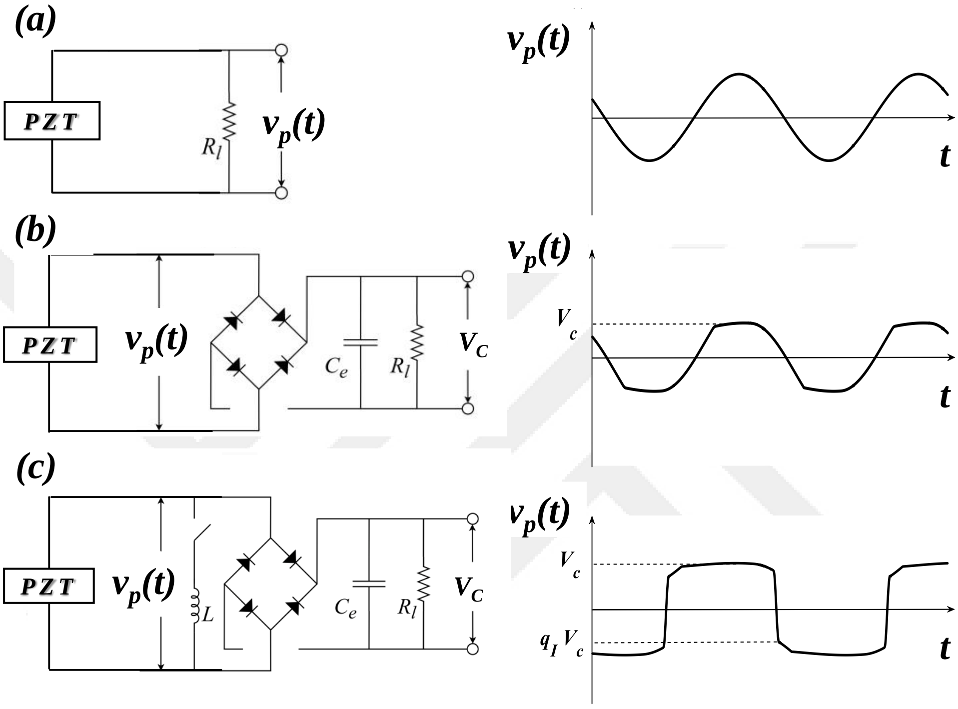

Figure 2.5: Piezoelectric voltage waveforms for (a) Resistor, (b) Rectifier, and (c) SSHI.

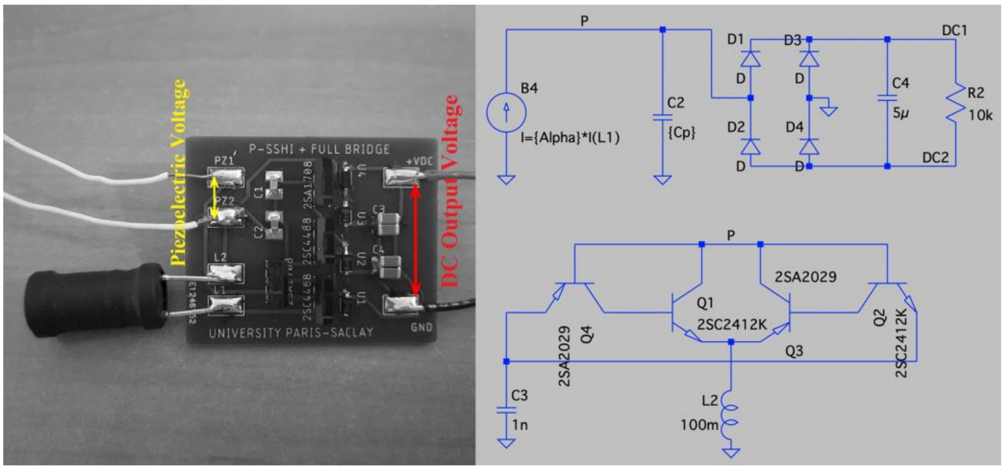

Figure 2.6: SSHI Circuit and its schematic.

2.4.2 Experimental validation for AC input- AC output

In the case of resistive load as harvesting circuit, a sine signal was swept over a frequency range of 40-115 Hz to measure the voltage frequency response function (FRF) of the system which was used to identify the modal damping ratios of the structure. The experimental voltage FRFs for any resistive load can be used to extract the modal damping ratios of the system [3]. The voltage FRFs of the harvester for AC input-AC output case with two resistive loads satisfying short circuit ($R_l = 100\ \Omega$) and open circuit ($R_l = 1\ M\Omega$) condition is shown in Figure 2.7.

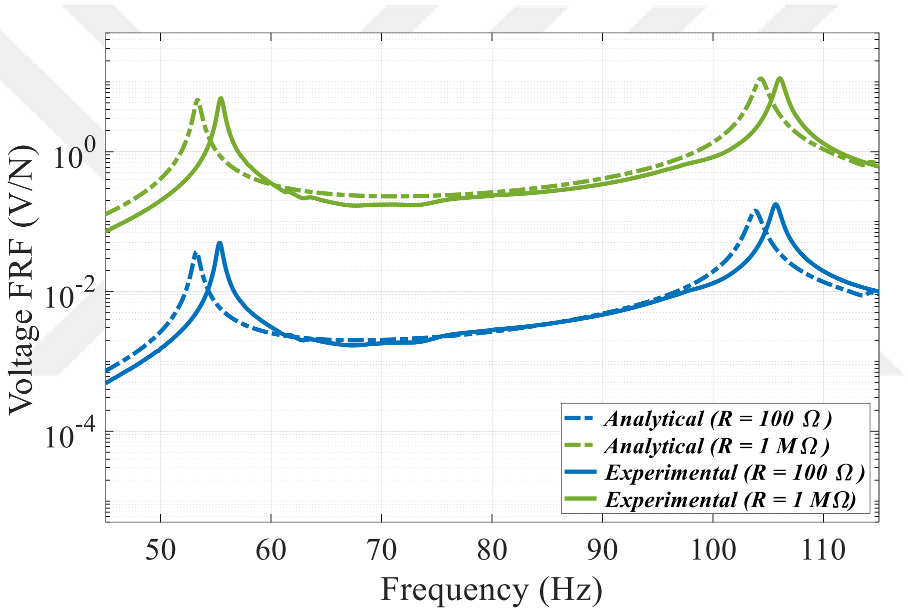

Figure 2.7: Comparison of analytical and experimental voltage FRFs for AC input-AC output.

As shown in Figure 2.7 the analytical voltage FRF prediction accurately matches with the experimental result. Comparing the experimental and analytical results, the predicted natural frequencies of the model have 3.8%, and 1.7% errors for the first and the second vibration modes of the system. It is worth mentioning that providing an ideal clamping condition for the plate structure in the experimental setup is difficult to achieve and any possible discrepancy in the boundary conditions can affect the modal parameters of the structure. Besides, the experimental room conditions specially the temperature can affect the natural frequencies of the plate [Cai et al., 2021]. Moreover, the material properties used in the analytical model are obtained from the standard tables of the aluminium alloy used in this experiment. However, there may be a difference between the actual values and the reported ones in the standards.

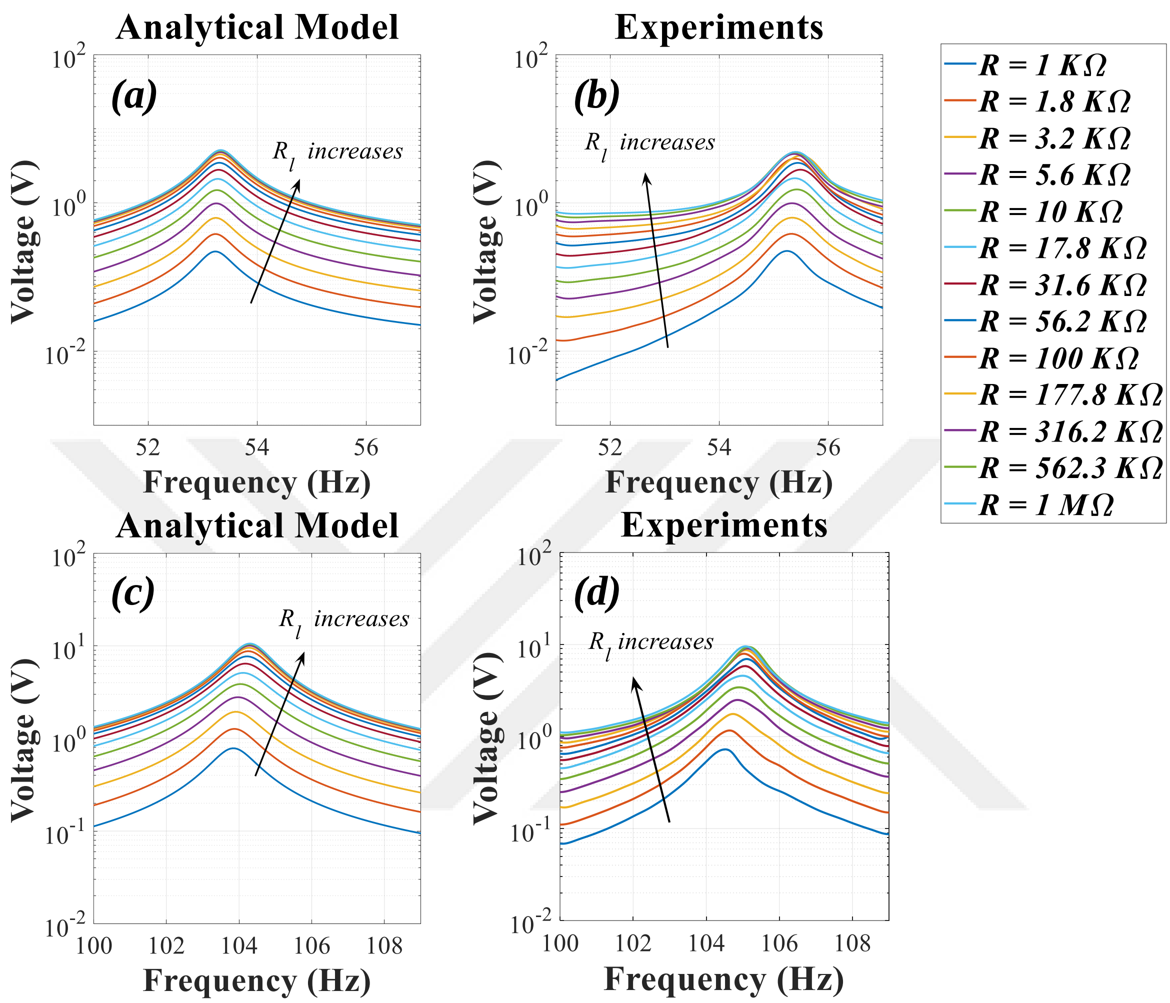

Figure 2.8: Analytical results and experiment data for DC output voltage of rectifier circuit under 1N excitation force.

2.4.3 Experimental validation for AC input-DC output with standard rectifier circuit

For the sake of comparison with the SSHI circuit, the DC response of PEH with rectifier circuit in frequency domain was obtained by sweeping the frequency of the harmonic excitation around two first natural frequencies of the harvester. The sweeping time of the swept sine signal has been kept long enough to capture the steady state response of the system and short enough to avoid huge experiment data (sweep-time = 180 (sec)). The voltage response of the rectifier for thirteen resistive loads ranging from 1 $K\Omega$ through 1 $M\Omega$ around two first natural frequencies of the plate was measured. The results of seven resistive loads are presented in Figure 2.8. Peak voltage response of the analytical model for several resistive loads has maximum error of 5.3% in the first vibration mode and 9% in the second vibration mode when compared with the experimental results. Although the voltage loss and the real diode behaviour are not included in the analytical model, the analytical model results reasonably follow the trend of the experimental voltage response where the voltage difference is less than 0.3 (V) and 0.9 (V) for the first and the second modes, respectively.

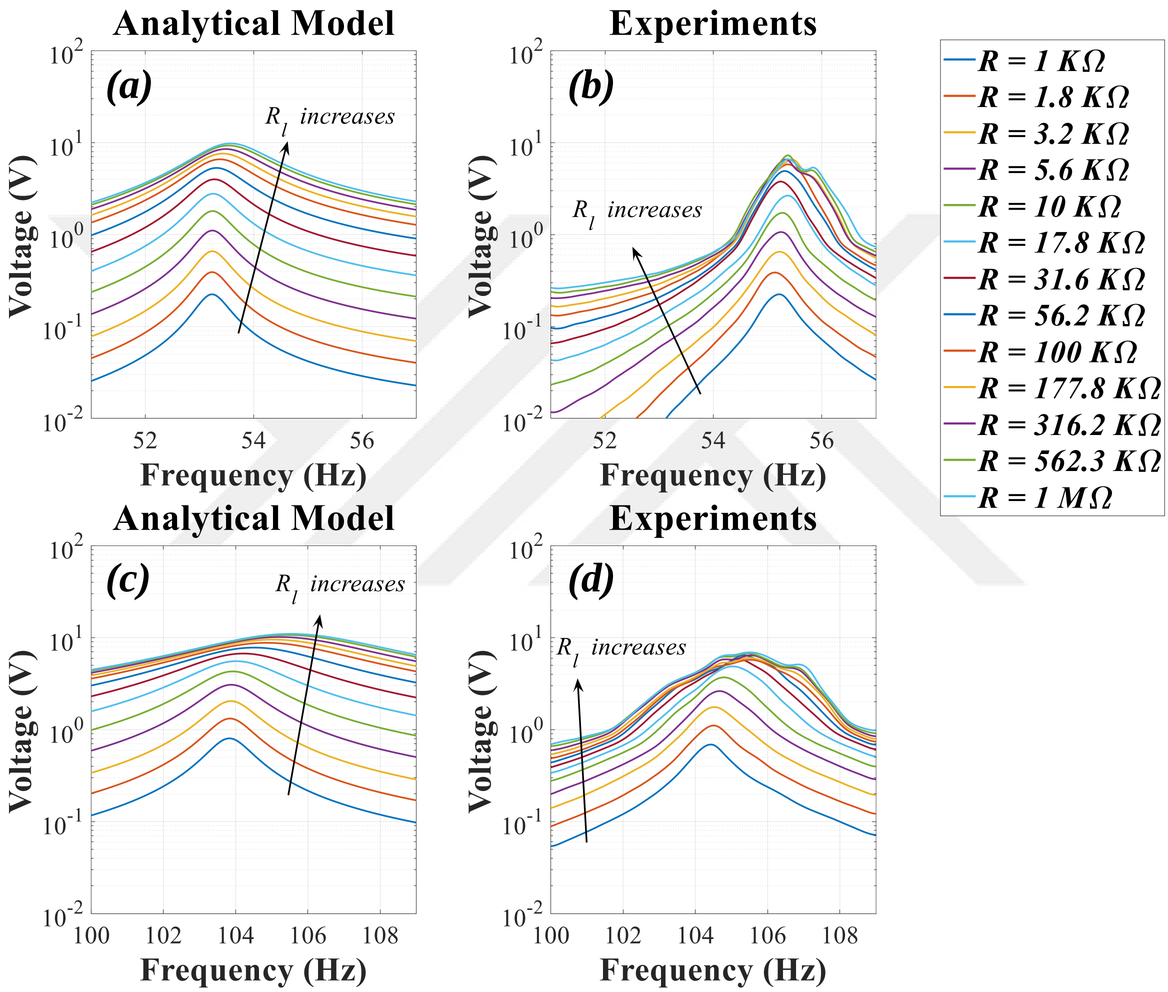

Figure 2.9: Analytical results and experiment data for DC output voltage of SSHI circuit under 1N excitation force.

2.4.4 Experimental validation for AC input-DC output with SSHI circuit

The aluminum plate with piezo patches was excited by a sine signal to obtain the harmonic response of the system for several resistive loads and assess the performance of the SSHI circuit when integrated with piezoelectric on the plate like host structure. The excitation frequency has been swept over a frequency range around the two first natural frequencies of the system considering an appropriate sweeping time (180 (sec)) which provides enough charge time for the smoothing capacitor and prevents large acquisition data due to high sampling rate. The quality factor of the SSHI circuit is 3.21. The output voltage of the SSHI circuit for thirteen resistive loads are measured and seven of them are compared with the analytical results in Figure 2.9. Experimental results show that the SSHI response resembles the response of the rectifier for the resistive loads of 1, 1.8, and 3.2 KΩ in the first mode, and for the resistive loads of 1 and 1.8 KΩ in the second mode. Studying the experimental piezoelectric voltage waveforms of the SSHI circuit which shows the behavior of the interface for different resistive loads (Figure 2.10 and Figure 2.11) comes up with the fact that the SSHI does not switch in low resistive loads since the piezoelectric voltage level is not sufficient to run the switching phenomena, and the SSHI circuit acts as a rectifier.

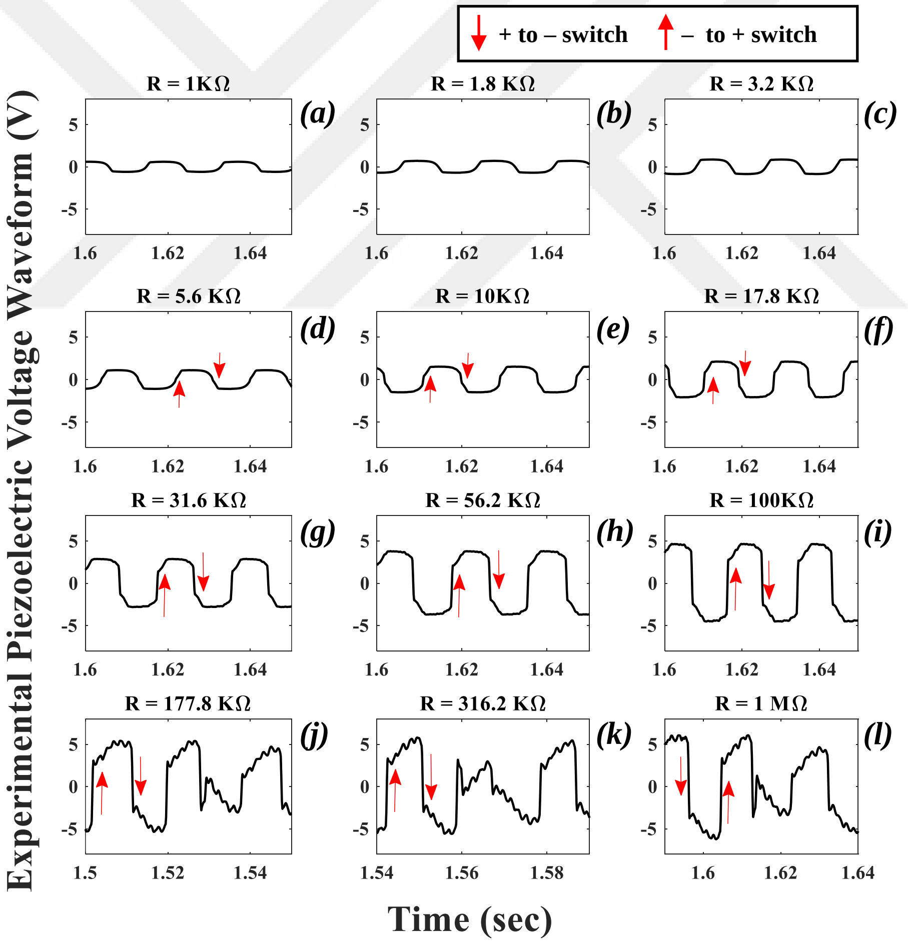

Figure 2.10: Experimental piezoelectric voltage waveforms (before the SSHI circuit) in the first vibration mode for different resistive loads. Indicate with (a)-(c) no switching … (d)-(i) single switching …, and (j)-(l) multiple switching.

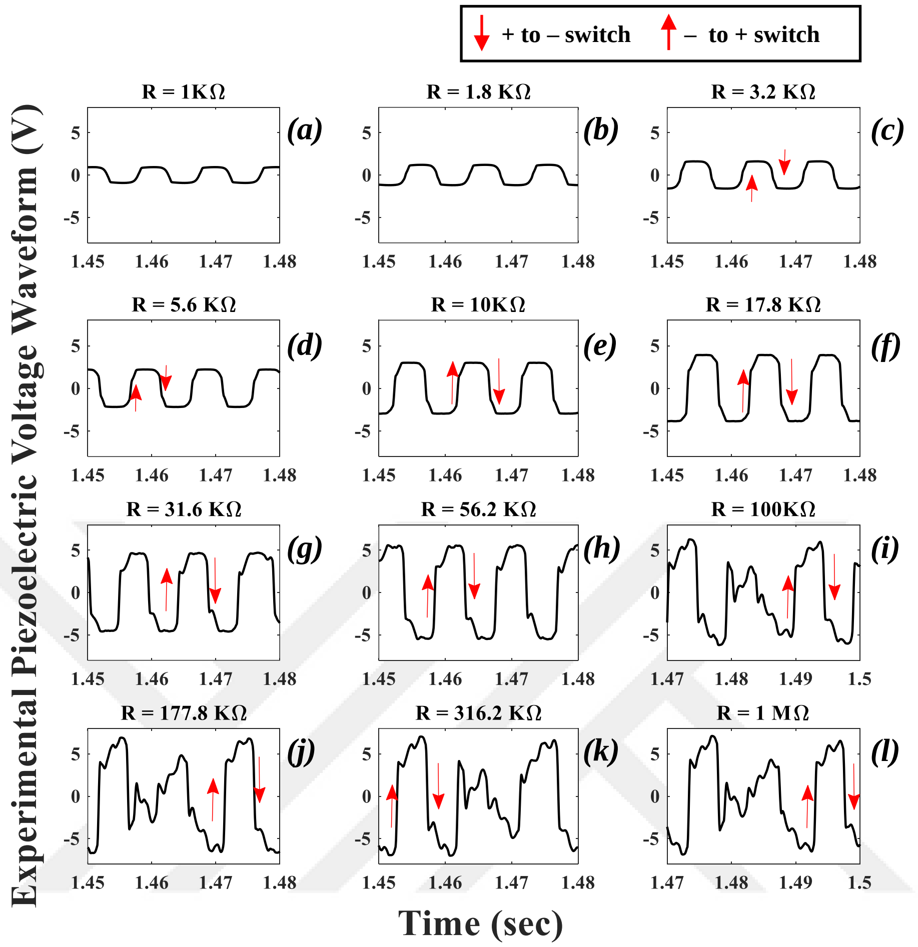

Figure 2.11: Experimental piezoelectric voltage waveforms (before the SSHI circuit) in the second vibration mode for different resistive loads. Indicate with (a) and (b) no switching … (c)-(h) single switching …, and (i)-(l) multiple switching.

It also can be seen in Figure 2.9 that the analytical model results follow the trend of the experimental data for the resistive loads between 5.6 KΩ and 100 KΩ in the first mode, and for the resistive loads between 3.2 KΩ and 56.2 KΩ in the second mode. In this range of resistive loads, the voltage difference between the analytical prediction and the experimental result for the peak voltage values are less than 0.55 (V) and 1.18 (V) in the first mode and the second mode, respectively. The voltage loss of the circuit components such as diodes and switching unit has not been included in the analytical model; however, the analytical model reasonably follows the trend of experimental results. The experimental piezoelectric voltage waveforms show that the SSHI circuit has a single switch in each half period of the vibration for this range of resistive loads which is the expected and the optimal behavior of the SSHI circuit.

Moreover, the voltage output of the SSHI for the resistive loads higher than 100 KΩ in the first mode, and for the resistive loads higher than 56.2 KΩ in the second mode does not follow the trend of the analytical prediction (Figure 2.9). The equivalent impedance of the harvesting circuit is based on the fundamental harmonic of the SSHI circuit [Liang & Liao, 2012a]; however, higher order harmonics for high resistive loads are significant and can be seen as ripples in the experimental piezoelectric voltage waveforms (Figure 2.10 and Figure 2.11). Therefore, the analytical model is not capable of predicting the trend of system behaviour for high resistive loads. The voltage difference between the analytical model and experiment is more than 1.75 (V) in first mode and more than 3.3 (V) in the second mode.

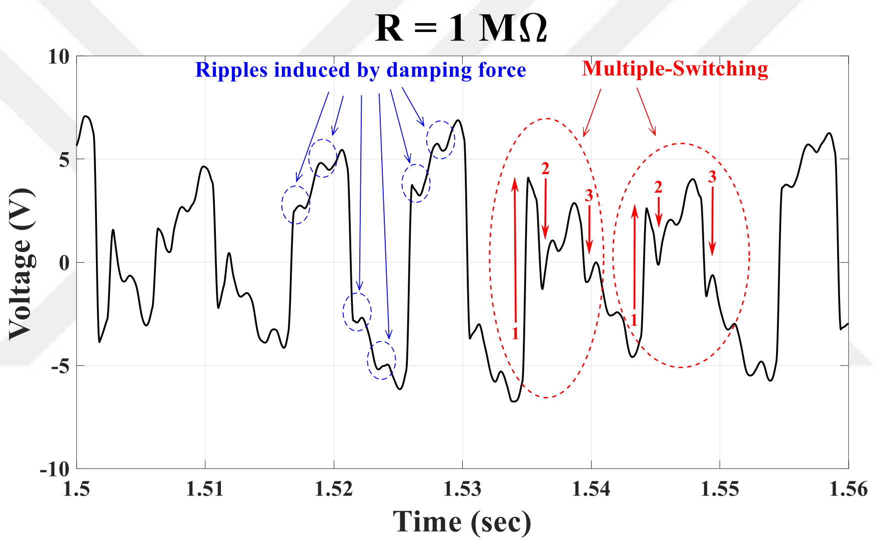

Figure 2.12: Multiple switching and ripple creation in piezoelectric voltage waveforms of second vibration mode (ω=55.2 Hz) for 1MΩ resistive load

It is worth noting that dense modal properties of the plate make the higher order harmonics become significant. The SSHI circuit affects the dynamic of plate by inducing a damping force which is considerable in higher voltage levels. When the frequency spectrum of the damping force coincides with the higher vibration modes of the plate, it induces an extra resonance to the dynamic of the plate and cause some ripples in the piezoelectric voltage waveforms (Figure 2.12). If the ripples are large enough, the multiple switching happens since the SSHI circuit detects them as local extrema and triggers the switch. Multiple switching dissipates a part of available energy and reduces the optimality of the SSHI interface. However, the multiple switching does not happen in optimum resistive loads. This behavior can be avoided or reduced by considering higher order harmonics of plate-like structure as a design parameter of the SSHI circuit and select appropriate inductance for the switching device.

Perfect performance of the SSHI circuit consists of switching the piezo-patch voltage at extremum displacement of the plate i.e., zero velocity of the plate. However, in practice, the switching process happens with a positive or negative time delay which can reduce the power output of the harvesters. The effect of switching delay depends on mechanical quality factor (Q_M) and electromechanical coupling factor (k^2) of the system . As it is shown in appendix (Figure 2.15), the SSHI device used in this study has positive switching delay. Considering the (k^2) and (Q_M) of the system, it can be concluded that the switching delay does not have significant effect on the power output of the harvesting system. Details of the switching delay and parameters of the system are available in the Appendix.

The experimental data and analytical prediction of the peak power output as a function of resistive loads for the SSHI circuit and the rectifier are compared in Figure 2.13. Analytical results illustrate that the optimum resistive load for rectifier in the first mode is 31.6 kΩ while it is 56.2 kΩ for SSHI circuit, and the respective average power output is 0.25 (mW) and 0.53 (mW) for rectifier and SSHI circuit, respectively. Also, the optimum resistance for the analytical power output of the SSHI and the rectifier in the second mode is 10 kΩ and 5.6 kΩ, respectively which leads to 1.86 (mW) and 1.51 (mW) power output, respectively. The analytical results show that the power output of the SSHI circuit at optimum resistance is 207% of the rectifier in the first mode and 124% in the second mode. On the other hand, the experimental data in the first mode shows that the maximum power output of the SSHI can be achieved at 31.6 kΩ where it is 17.8 kΩ for the rectifier. The maximum power output obtained from experiment in the first mode for the SSHI is 0.4779 (mW) while it is 0.26 (mW) for the rectifier. Besides, the maximum power output of experimental results in the second mode is 1.58 (mW) for SSHI circuit with 10 KΩ resistive load and 1.177 (mW) for rectifier with 17.8 KΩ resistive load. The Experimental power output of the SSHI circuit is 183% and 134% of the rectifier for mode one and mode two, respectively. The analytical results and experimental data for the first vibration mode show that the SSHI circuit improves the power output of the harvester for all resistive loads except where it is not active. Although the power output of the harvester in the second vibration mode is improved by the SSHI circuit in optimum resistive load, the analytical and experimental results show that the SSHI circuit is not effective for relatively high resistive loads in second mode. The analytical model is only capable of predicting the linear regime where single switching at each half period of vibration occurs, but the model cannot predict the nonlinearities of experimental setup at high resistive loads. The multiple switching reduces the power output of the system which is more visible at second vibration mode. The power reduction due to multiple switching at second vibration mode reduces the performance of the SSHI circuit even lower than standard rectifier.

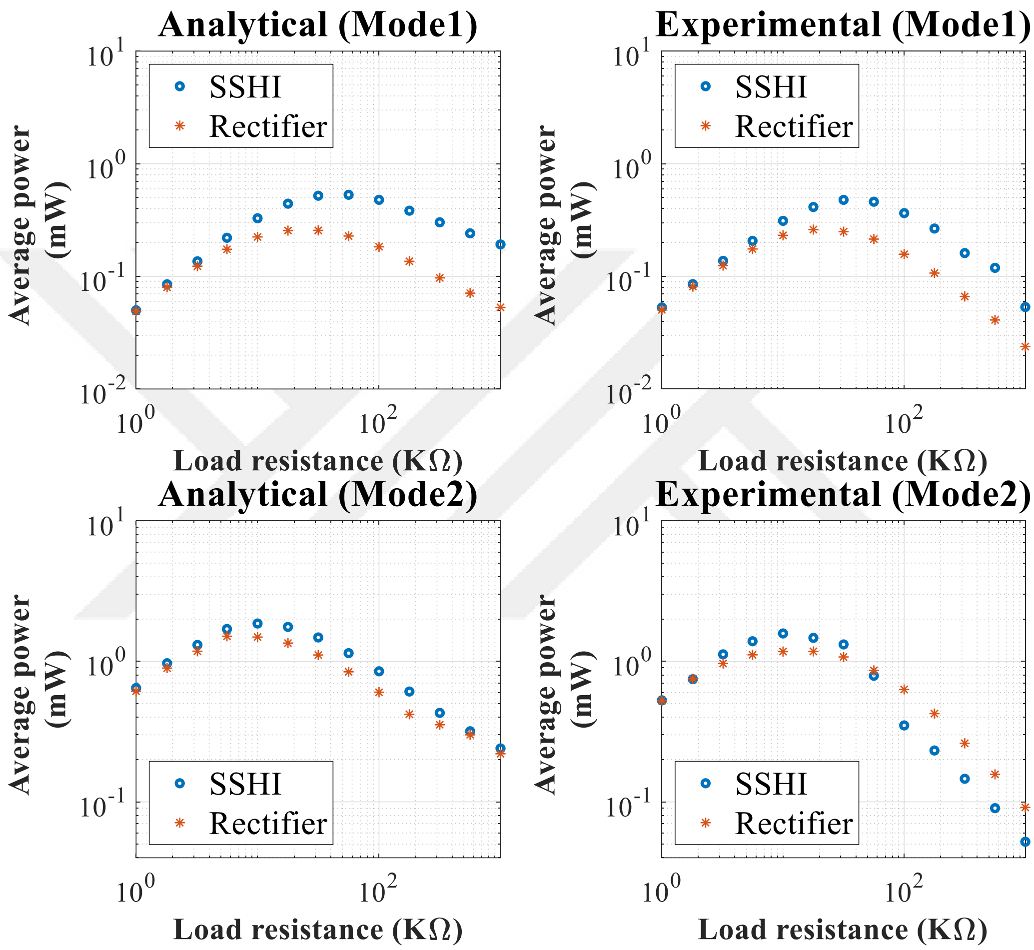

Figure 2.13: Analytical and experimental results for average power output of the SSHI and rectifier circuits.

A comprehensive experiment has been performed to assess the behavior of the SSHI circuit for different input force levels, and resistive loads. Thirteen resistive loads between 1 KΩ and 1 MΩ with logarithmic increments and force levels, namely 0.5, 65, 82, 1, and 1.15 (N), have been considered to study the response of the piezoelectric energy harvester integrated with the SSHI circuit. The DC voltage output of the PEH in the first vibration mode (Figure 2.14a) and the second vibration mode (Figure 2.14b) show that the higher the input gain and the resistive load, the higher the DC voltage output. However, this trend is more visible in single switching areas, and the rate of voltage increase is dropped in multi-switching zone which shows that the performance of the SSHI circuit is not efficient. Therefore, multi-switching should be avoided to make the SSHI circuit reach its optimal performance. Besides, the DC output voltage level of 1.5 V is a threshold for triggering the switch, where the DC voltage levels higher than 5V experience the multi-switching. Regarding the power output of PEH, the optimum resistive loads of different force inputs are available in Figure 2.14c and Figure 2.14d for mode 1 and mode 2, respectively. The optimum resistive load of almost all the cases in the first mode is 31.6 KΩ, and in the second mode is 10 KΩ.

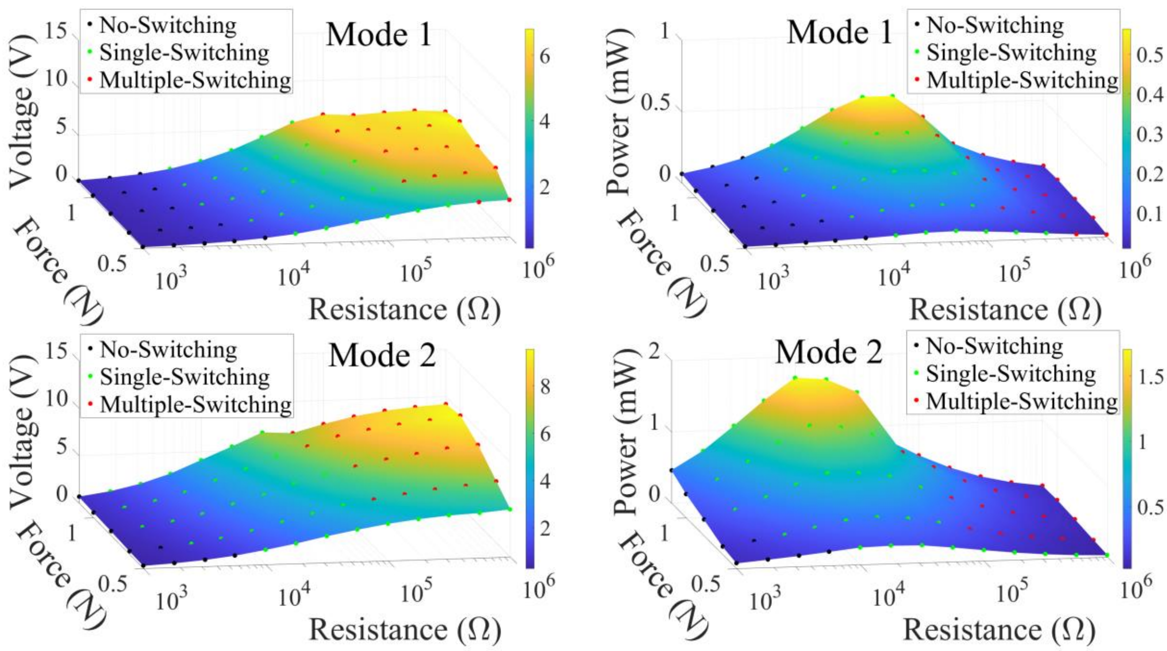

Figure 2.14: DC voltage and power output of the SSHI circuit for different input force levels and resistive loads. (a) and (c) first vibration mode (ω = 55.2 Hz), (b) and (d) second vibration mode (ω = 104.5 Hz).

2.5 Conclusion

In this chapter, an analytical model was developed to predict the behavior of a piezoelectric energy harvester on a thin plate integrated with an SSHI circuit. Structural analysis was performed based on Rayleigh-Ritz method to obtain an electromechanical model of the plate with PEH, and the equivalent impedance approach was used to provide a closed-form solution for the system. The steady-state voltage output of the piezoelectric energy harvester for a range of resistive loads around first and second natural frequencies were predicted by analytical solution and validated by the experimental data where the SSHI circuit had single switching in each half period of the vibration. A comprehensive analysis of the SSHI circuit behavior on the plate for different force inputs and resistive loads was investigated and presented. Using a 2D electromechanical plate, multi-switching of the SSHI circuit in higher piezoelectric voltage levels was observed. Multiple switching increased the energy dissipation of the harvesting circuit; thus, the output voltage of the harvester dropped drastically when compared to the analytical prediction. Furthermore, the peak power output of the SSHI circuit as a function of resistive load was compared with the rectifier for the first two vibration modes of the plate to assess the functionality of the SSHI circuit in multimodal energy harvesting applications. It has been demonstrated that the SSHI circuit improves the power output of the PEH for both vibration modes in optimum resistive loads. Practically, the maximum power outputs of the SSHI circuit for the first and the second vibration modes were 183% and 134% of the maximum power outputs of the rectifier, respectively.

Despite improvements on maximum power output of the piezoelectric energy harvester by the SSHI circuit, undesired behavior of the switching device is reported when the PEH is attached to the plate-like structure. The developed equivalent impedance model can predict the linear regime of SSHI circuit, where the single switching occurs at each half period of vibration. At high resistive loads leading to higher voltage levels, higher modal harmonics of the host plate are coupled with switching dynamics of SSHI circuit. In order to avoid multiple switching behavior of the SSHI circuit, it is worthful to consider the higher order harmonics of the plate-like structure as a design parameter. The value of inductor on switching device should satisfy the synchronized switching criteria as well as avoiding the multiple switching behavior of SSHI circuit when integrated with plate-like structures. Adding filters in the peak voltage detector of the switching device is another approach that could be investigated to avoid performance drop resulting from multiple switching.

2.6 Appendix

The ideal performance of the SSHI circuit is the triggering the switch at the zero velocity of the PEH. Yet, in practical applications, there is a negative or positive time delay between the actual occurrence of zero velocity and the inversion. Negative switching delay corresponds to the triggering of the switch before reaching the zero velocity, where positive delay refers to the switching after the zero velocity [Lallart et al., 2011]. It is proved in [Lallart et al., 2011] that the power reduction level depends on the sign of delay, length of delay, and figure of merit (FoM). Figure of merit is defined as the product of mechanical quality factor (Q_M) and the global electromechanical coupling factor (k^2). The mechanical quality factor depends on the modal damping ratio (ζ_{mn}) and is defined as:

$$Q_M = \frac{1}{2\zeta_{mn}} \tag{2.20}$$

The electromechanical coupling factor can be calculated by

$$k^2 = 1 - \frac{\omega_{sc}^2}{\omega_{oc}^2} \tag{2.21}$$

where the ω_{sc} and ω_{oc} represent the short circuit and open circuit resonance frequencies.

The voltage and velocity waveforms of piezo patch (Figure 2.15) illustrate that the SSHI circuit has positive switching delay which does not have significant effect on output power for a large range of time delay. The power drop of the harvester has been studied by Lallart et al. [Lallart et al., 2011] for five values of FoM varying from $FoM = 0.1877$ as weakly coupled and $FoM = 3.1845$ as strongly coupled harvesters, and it has been shown that the power drop in the positive switching delay decreases by increasing the FoM. The parameters of the energy harvester integrated with the SSHI circuit for the first and the second vibration modes are available in Table 2.2.

Comparing the $FoM = 0.982$ and $FoM = 1.81$, respectively, for the first and the second vibration modes of the system with the results of Lallart et al. [Lallart et al., 2011], and considering the positive time delay ratio less than 0.03 of vibration period for both modes, the power drop of the harvester due to the switching delay can be negligible for the SSHI circuit.

Table 2.2: The parameters of the energy harvester integrated with the SSHI circuit.

Parameter	Mode 1	Mode 2
ω_{sc} (Hz)	53.22	103.81
ω_{oc} (Hz)	53.51	104.84
ζ_{mn}	0.0055	0.0054
k^2	0.01081	0.01955
Q_M	90.9	131.57
FoM	0.982	1.810

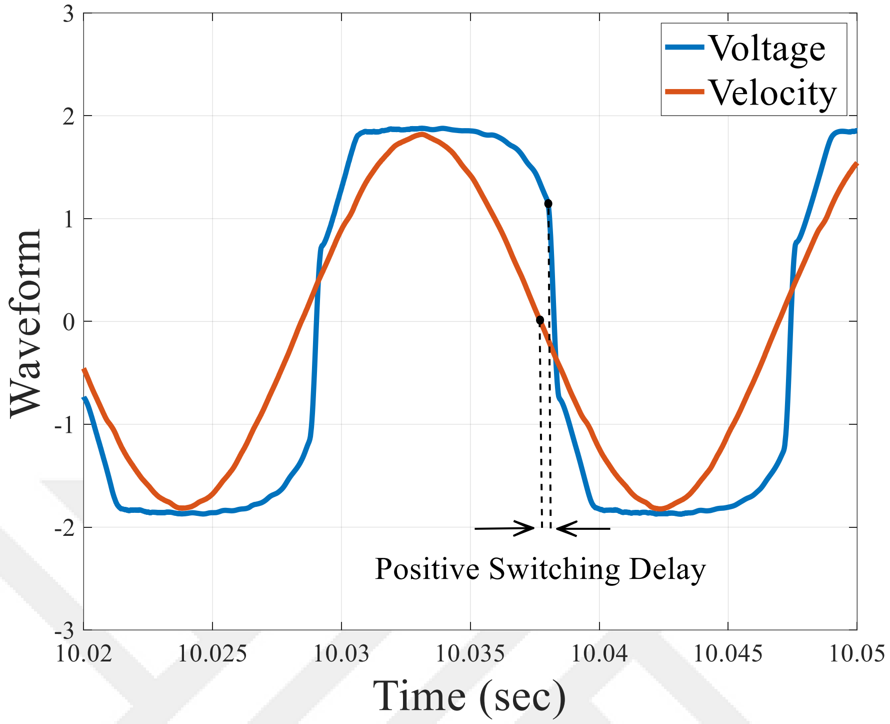

Figure 2.15: Piezoelectric voltage and velocity waveform in the first resonance frequency (ω = 55.2 Hz).

CHAPTER 3

EXPERIMENTAL SYSTEM IDENTIFICATION FOR EQUIVALENT CIRCUIT MODELING OF PIEZOELECTRIC ENERGY HARVESTERS

3.1 Introduction

In this chapter, a robust and straightforward methodology is introduced to identify the parameters of multi-modal ECM based on electromechanical admittance measurements of the electromechanical system. Despite all the efforts on obtaining the parameters of an equivalent circuit for a piezoelectric transducer [Guan & Liao, 2009; Hagmann, 2019; Sobral & Santos, 2013], a comprehensive and practical method has not been reported in the literature to identify the multi-modal equivalent circuit model of the piezoelectric energy harvesters from experimental measurements. This chapter presents a method for determining the ECM parameters as well as identifying the equivalent voltage sources corresponding to the input force. The identification of R_n, L_n, C_n, and C_0 is independent of the force location, and it is conducted by performing electrical excitation using impedance analyzer where there is no mechanical excitation. On the other hand, the identification of the equivalent voltage sources of each vibration mode depends on the force location since the voltage sources are representing the contribution of the input force in modal coordinate. The method allows for system identification of any low-damped piezoelectric harvesting system regardless of the structural geometry and any prior knowledge of the modal, mechanical, and electrical properties of the system. To validate the proposed method, three case studies were conducted. The first case study involved a single piezo-patch on a fully clamped thin plate integrated with a resistive load. In the second case study, multiple piezo-patches were connected in series or parallel on a thin plate, also integrated with a resistive load. Lastly, the third case study focused on series-connected piezo-patches on a fully clamped thin plate, which were integrated with a standard rectifier. First, the parameters of ECM, as well as equivalent voltage sources for the vibration modes were identified using the measured admittance and charge frequency response of the energy harvesting setup. Then the model was developed in LTspice software to obtain the output voltage of the model. In parallel, experiments were conducted to obtain the voltage response of the energy harvesting setup under the harmonic point force using a vibration shaker. Comparing the experimental results with the results of the equivalent circuit model shows that the proposed approach accurately predicts the electromechanical behavior of the piezoelectric energy harvester.

3.2 Multi-modal equivalent circuit model

As it is shown in Figure 3.1, the multi-modal ECM has different circuit elements which can be categorized in three main sections i.e., piezoelectric capacitance (C_0), parallel connected branches of LCR (inductance-capacitance-resistance in series) circuit, and equivalent voltage sources, which represent the electrical behavior, mechanical properties, and excitation input of the system, respectively. Each LCR branch corresponds to a vibration mode of the structure.

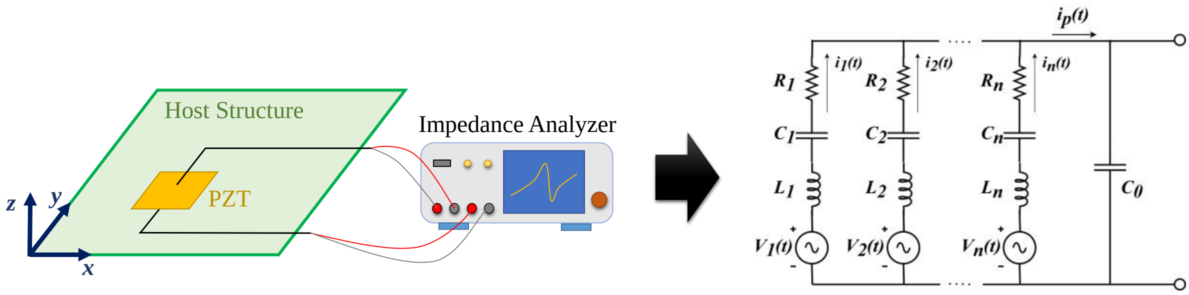

Figure 3.1: Multi-mode equivalent circuit model of a piezoelectric energy harvester.

The governing equations of motions of the piezoelectric plate energy harvesting system around resonant frequency can be given by [Liao & Liang, 2018]:

$$M\ddot{z}(t) + D\dot{z}(t) + Kz(t) - \theta v_p(t) = f(t) \tag{3.1}$$

$$\theta z(t) + C_0 v_p(t) = q_l(t) \tag{3.2}$$

where $z(t)$, $v_p(t)$, $f(t)$, and $q_l(t)$ are, respectively, displacement of structure, piezoelectric voltage, force input and charge passing through terminal load. M, K, D, and θ denote the equivalent mass, short-circuit stiffness, mechanical damping, and coupling coefficient, respectively. Dividing equation (3.1) by θ and multiplying first, second, and third terms by $\frac{\theta}{\theta}$, it can be rearranged as [Liao & Liang, 2018]:

$$\frac{\mathrm{M}}{\theta^2}\frac{d^2}{dt^2}\big(-\theta z(t)\big) + \frac{\mathrm{D}}{\theta^2}\frac{d}{dt}\big(-\theta z(t)\big) + \frac{\mathrm{K}}{\theta^2}\big(-\theta z(t)\big) - v_p(t) = \frac{f(t)}{\theta} \tag{3.3}$$

where $-\theta z(t)$ corresponds to the piezoelectric charge response. The equivalent mechanical terms of the ECM can be estimated as $L = \frac{M}{\theta^2}$, $R = \frac{D}{\theta^2}$, and $C = \frac{\theta^2}{K}$ by the analogy between a second-order circuit's equations and equation (3.3) [Liao & Liang, 2018]. Here, an experimental method based on electromechanical admittance is proposed to determine the parameters of a multi-mode ECM of the piezoelectric energy harvester from the experimental setup. The equivalent circuit modeling procedure consists of determining the following parameters:

- Internal capacitance of piezoelectric (C_0).
- Equivalent system parameters (LCR) for each vibration mode of the piezoelectric energy harvester.
- Voltage source for each LCR branch.

The proposed method is developed by measuring the electromechanical admittance of the piezoelectric transducer; therefore, an impedance analyzer device can be used to measure the admittance of the PEH. An impedance analyzer measures the impedance or admittance of the circuit based on the AC voltage across the circuit and the current passing through it. The ratio of current to voltage is defined as admittance of the circuit.

3.3 General procedure of identifying the experimental ECM

In this section, the steps of identifying the parameters of the ECM through experimental measurements are summarized as follows (see Figure 3.2 showing the steps as a flowchart).

- Perform electrical excitation using an impedance analyzer to identify C_n, L_n, R_n, and C_0.

- Measure the admittance of PEH for a frequency range to determine the resonance frequencies of the system.

- Measure the admittance of PEH around each resonance frequency such that the resonances and antiresonances are captured during the measurement.

- Determine the equivalent piezoelectric patch capacitance (C_0).

- Identify the parameters of each LCR branch for the corresponding vibration mode.

- Perform mechanical excitation to identify the voltage source (V_n) by attaching the shaker to the setup.

- Measure the output voltage FRF of the system for the desired harmonic point force in open circuit condition.

- Calculate the charge response of the system using the open circuit voltage FRF and piezoelectric capacitance (C_0).

- Identify the equivalent voltage source for each vibration mode.

It is worth noting that the admittance of the ECM around nth natural frequency can be estimated as [Priya & Inman, 2008]:

$$Y = j\omega \left(C_0 + \frac{C_n}{1 + C_n\omega(jR_n - L_n\omega)} \right) \tag{3.4}$$

where C_0, C_n, L_n, R_n, and ω are, respectively, the internal capacitance, the equivalent capacitance, inductance, resistance, and vibrating frequency of the piezoelectric at nth vibration mode of the structure. Damped admittance (Y_d) and motional admittance (Y_{mot}) are introduced as $Y_d = j\omega C_0$, and $Y_{mot} = j\omega \left(\frac{C_n}{1+C_n\omega(jR_n - L_n\omega)} \right)$, respectively. The details of the procedure to obtain the ECM from measured admittance of the PEH will be explained in the following sections.

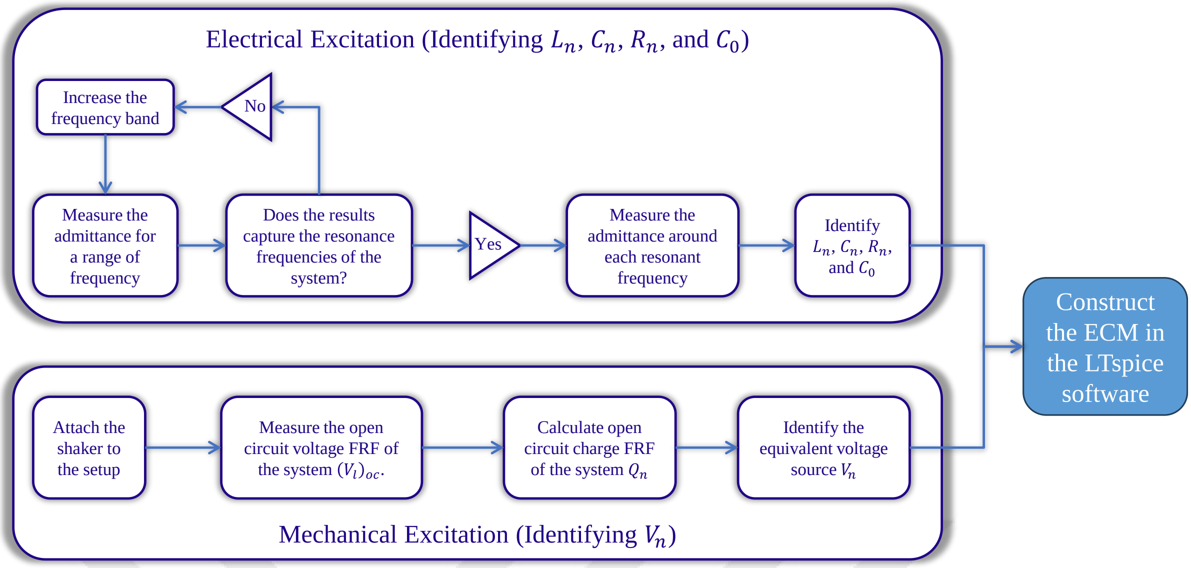

Figure 3.2: Flowchart for identifying the ECM of piezoelectric energy harvester through experimental method.

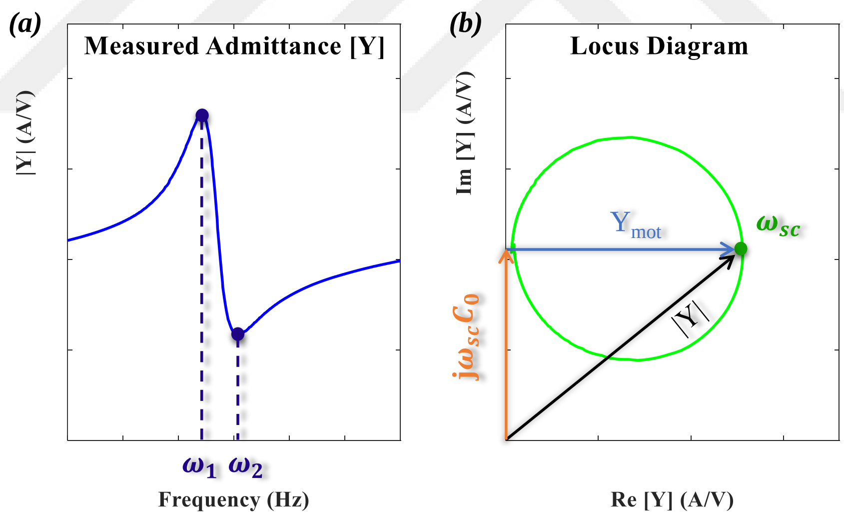

Figure 3.3: Piezoelectric energy harvester admittance (a) frequency domain (b) Locus diagram.

3.3.1 Determining the equivalent piezoelectric patch capacitance (C_0)

The piezoelectric capacitance C_0 can be determined by considering the admittance (Y) locus diagram around the resonant frequency of the harvester. Total admittance of a PEH measured by an impedance analyzer around resonance frequency is shown in Figure 3.3 and it is the sum of the motional admittance (Y_{mot}) and the damped admittance (Y_d). C_0 can be obtained at short circuit natural frequency $(\omega_{sc})_n = \sqrt{\frac{1}{C_n L_n}}$ in which the motional admittance (Y_{mot}) is maximum and it is a real number. The imaginary part of the total admittance (Y) at this frequency is equal to the damped admittance (Y_d) which corresponds to the admittance of the C_0 [Ikeda, 1990].

3.3.2 Identifying the equivalent mechanical components (*L_n, C_n, and R_n)*

Equivalent mechanical components of the ECM represent the dynamic properties of the PEH. Each vibration mode of the system is modeled as a branch of a second-order circuit which is in parallel with other vibration modes. Considering equation (3.4) at nth short circuit resonant frequency, the admittance of the equivalent resistance (Rn) is equal to the real part of the total admittance (Y). The quality factor of the ECM can be determined by $Q_n = \frac{(\omega_{sc})_n}{\omega_2 - \omega_1} = \frac{1}{R_n}\sqrt{\frac{L_n}{C_n}}$. Consequently, the inductance (Ln) can be calculated by the value of the resistance and the frequencies at which the total admittance is maximum (ω_1) and minimum (ω_2). Knowing the short circuit natural frequency $(\omega_{sc})_n$ and the inductance (L_n), capacitance (C_n) can be obtained [Priya & Inman, 2008]. The parameters can be identified by applying the following equations:

$$R_n = \frac{1}{max[Re(Y)]} \tag{3.5}$$

$$L_n = \frac{R_n}{\omega_2 - \omega_1} \tag{3.6}$$

$$C_n = \frac{1}{L_n.(\omega_{sc})_n{}^2} \tag{3.7}$$

3.3.3 Determining equivalent voltage sources (*V_n)*

The equivalent voltage source of the nth branch represents the input force for the nth vibration mode of the PEH. Yang and Tang [Yang & Tang, 2009] determined the equivalent voltage sources considering short circuit condition, where the output voltage of the piezoelectric becomes zero i.e., $v_p(t) = 0$. Fourier transform of equation (3.3) for short circuit condition at resonant frequency is as follows [Yang & Tang, 2009]:

$$V_n = R_n\, j\omega_n\, Q(j\omega_n) \tag{3.8}$$

where R_n is the equivalent resistance of the ECM, ω_n is the nth resonance frequency of the system, and $Q(j\omega_n)$ is the piezoelectric charge response at nth resonant frequency for short circuit condition. However, practically, measuring the $Q(j\omega_n)$ for short circuit condition is a hard practice. Instead, the experimental output voltage FRF of the PEH setup for open circuit condition $(V_l)_{oc}$ can be used to determine the charge response of the PEH for a unit harmonic force since all the piezoelectric charge is stored in the piezoelectric capacitor (C0) at open circuit condition and there is no output charge flow i.e., $-\theta z(t) = C_0 v_p(t)$ and $q_l(t) = 0$. The charge response of the piezoelectric to the unite input force is shown in Figure 3.4 and can be obtained from the open circuit voltage response as follows:

$$Q = C_0 . (V_l)_{oc} \tag{3.9}$$

The sign of voltage sources for each vibration mode is the sign of imaginary part of charge FRF (Q) at each natural frequency (Figure 3.4).

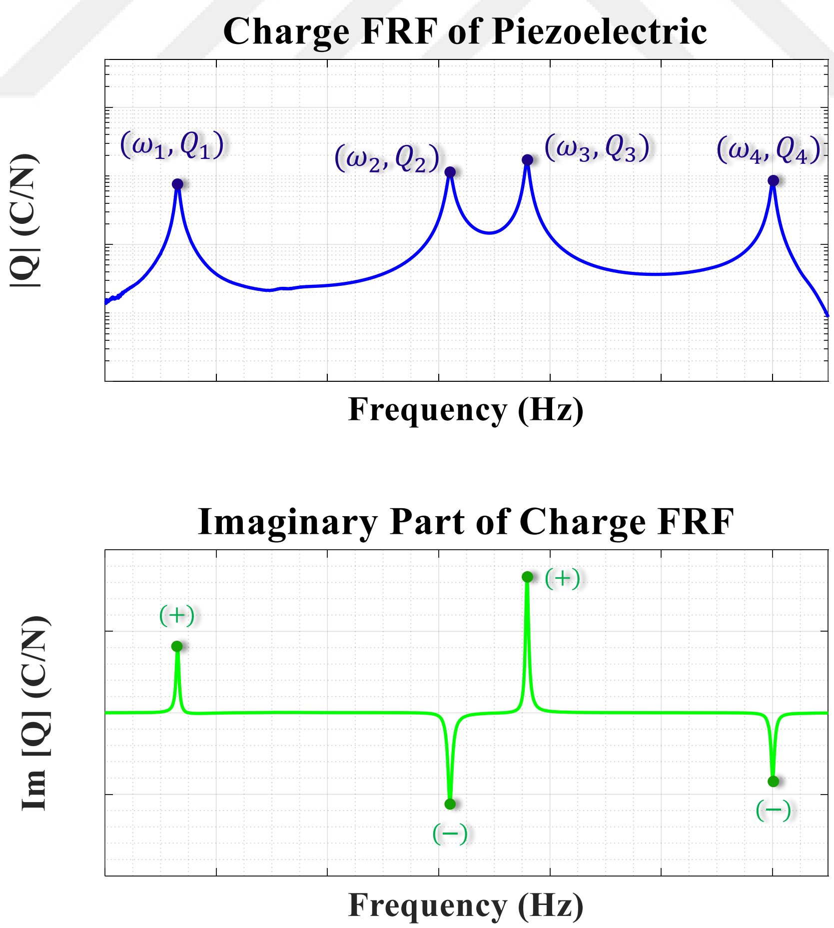

Figure 3.4: Charge response of a piezoelectric patch to force input.

3.4 Experimental validation of the ECM

The validation of the proposed method for equivalent circuit modeling has been investigated with a fully clamped (CCCC) aluminum plate as the host structure. Three piezo-patch harvesters (T105-A4E-602 manufactured by Piezo Systems, Inc.) were attached to the host structure, where the patch in the center of the plate has been short circuited to minimize the backward effect of the patch and other two patches were used for the validation of the method. The experimental setup of the piezoelectric energy harvester is shown in Figure 3.5.

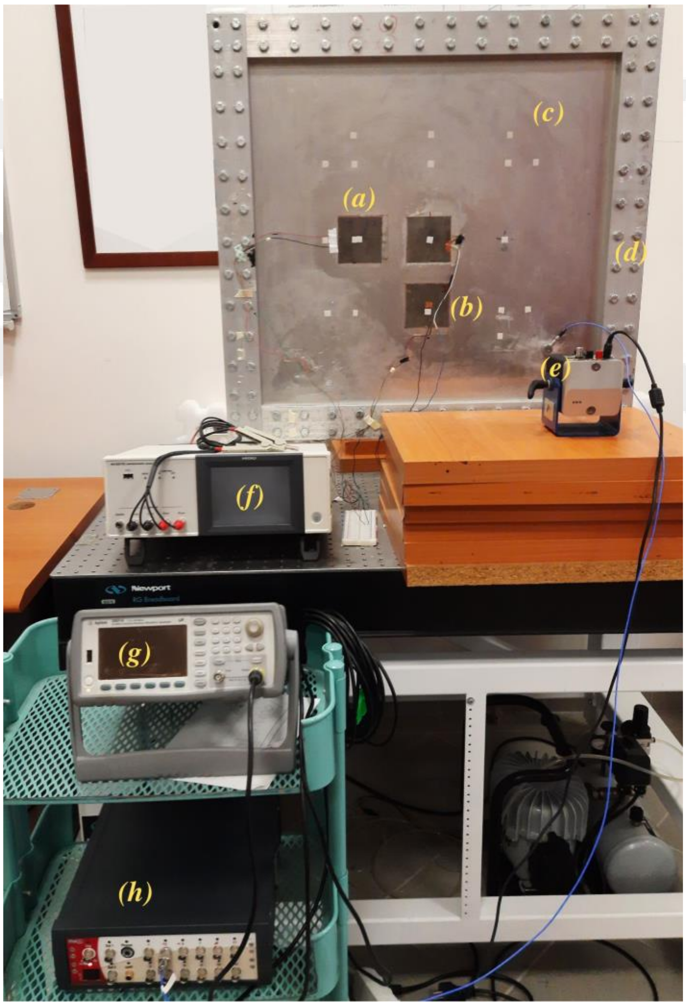

Figure 3.5: Experimental setup: (a) PZT-1; (b) PZT-2; (c) aluminium plate; (d) clamping frame; (e) shaker and a force transducer; (f) impedance analyzer; (g) signal generator; (h) data acquisition unit.

Three cases have been considered to assess the proposed method namely, single PEH integrated with resistive load, multiple piezoelectric patches connected in series/parallel integrated with a resistive load, and series connected multiple piezoelectric patches integrated with standard rectifier. First, the ECM of each piezoelectric patch was identified by measuring the admittance of piezoelectric with impedance analyzer where there is no shaker attached to the setup. The identified ECM was developed in LTspice software to obtain the voltage response of the model. In parallel, the voltage frequency response of the system under the effect of point force is measured. The details of the procedure for each case are explained in the following sections.

3.4.1 Case I: Validation with a piezoelectric patch integrated with resistive load

The ECM identification process consists of two main stages. First, the shaker was not attached to the plate and the admittance of the piezoelectric energy harvester was measured by the impedance analyzer (HIOKI IM3570). Then, the shaker was attached to the plate and the charge response of the system to a point force was measured.

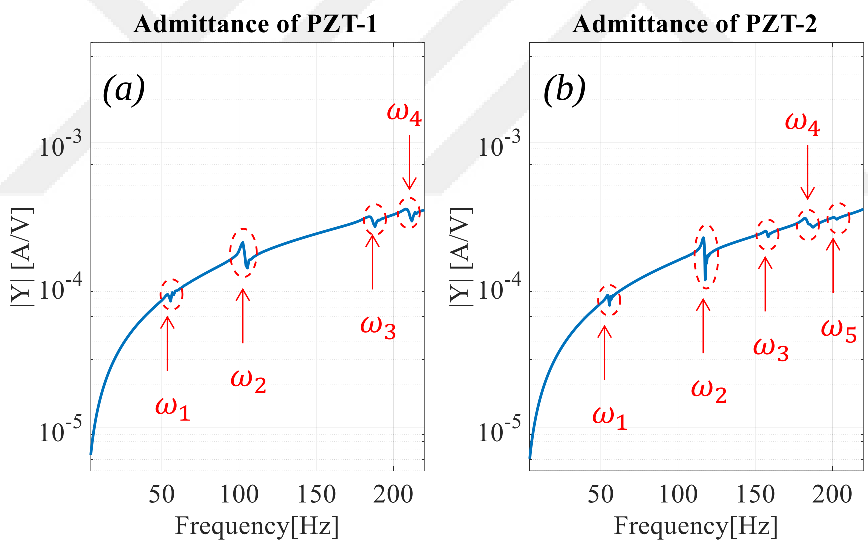

Figure 3.6: Admittance of (a) PZT-1 (b) PZT-2 for the frequency range of 0 – 230 Hz.

Before starting the measurements, it is mandatory to identify the resonance frequencies of the harvester. In order to show that the methodology is independent of the patch location, the admittance of the PZT-1 and PZT-2 have been measured in the range of 4 – 230 Hz as shown in Figure 3.6. The magnitude of the measured admittance tends to increase by the frequency which can be also observed in equation (3.4). Resonances and antiresonances are found in wide-band frequency sweeps. Then the natural frequency of the structure and LCR parameters for each vibration mode are identified by a narrower frequency sweep around each resonant peak. The result shows that PZT-1 captures four resonances around 54 Hz, 103 Hz, 185 Hz, and 205 Hz where PZT-2 captures five resonances around 54 Hz, 115 Hz, 160 Hz, 185 Hz, and 205 Hz.

Determining the resonance frequencies, the admittance of each PEH is measured around each resonance frequency. Using equations (3.4) through (3.6), the parameters are identified by frequency response and locus diagram of the piezoelectric admittance for several resonance frequencies. Figure 3.7 and Figure 3.8 illustrate the amplitude and locus of the measured admittance around the resonance frequencies, and the identified parameters for the equivalent circuit model of the PZT-1 and PZT-2, respectively.

The final step is to identify the equivalent voltage source for each vibration mode which represents the modal force input of the system. In order to measure the dynamic force input of the system, a force transducer (PCB 208C02) was used at the tip of the shaker, located at 0.087 m from the bottom right corner of the plate in both x and y directions. A sine signal ranging from 40 to 230 Hz was used to determine the steady state voltage FRF of each piezoelectric patch under open circuit conditions for AC input-AC output case. The voltage FRF has been measured separately for each piezoelectric patch where other piezoelectric patches are short circuited. The charge frequency response of the system was determined using equation (3.8), and equation (3.7) was then used to identify the amplitude of equivalent voltage sources. The sign of the equivalent voltage source for each vibration mode is indicated by the sign of the imaginary part of the charge FRF, as shown in Figure 3.4.

The LTspice software has been used to construct the ECM of each harvester and obtain the voltage frequency response of the model. Besides, the output voltage FRF of each harvester for the resistive loads 1 KΩ, 10 KΩ, and 1 MΩ were obtained to validate the equivalent circuit model of the harvester. The output voltage FRF of the model for PZT-1 and PZT-2 are compared with experimental results in Figure 3.9 and Figure 3.10, respectively, which shows that the identified ECM from the experiment can accurately predict the behaviour of the piezoelectric energy harvester around resonance frequencies. The experimental results show that each piezo patch misses some vibration modes due to the location of the patch. If the piezoelectric patch is located at nodal lines of a vibration mode of the host structure, the measured admittance does not have resonance and antiresonance where the ECM cannot be determined.

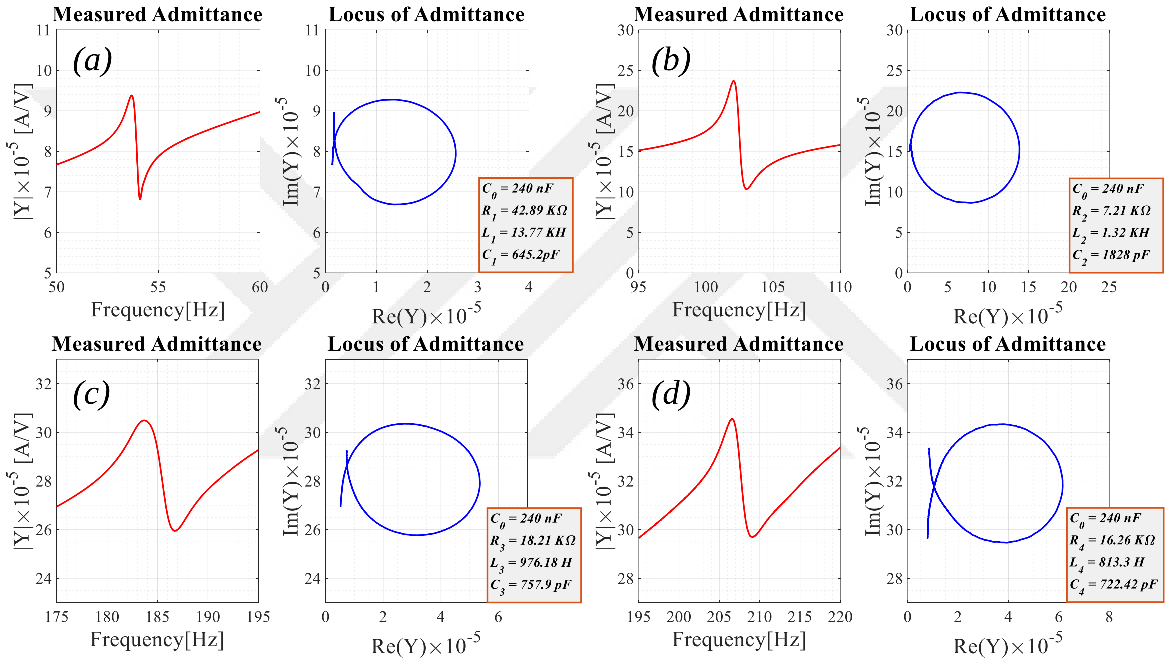

Figure 3.7: The parameters of the ECM for (a) first (b) second (c) third (d) fourth vibration mode identified by measuring the admittance of PZT-1. Red lines are the measured amplitude of admittance. Blue lines are the locus diagram of measured admittance.

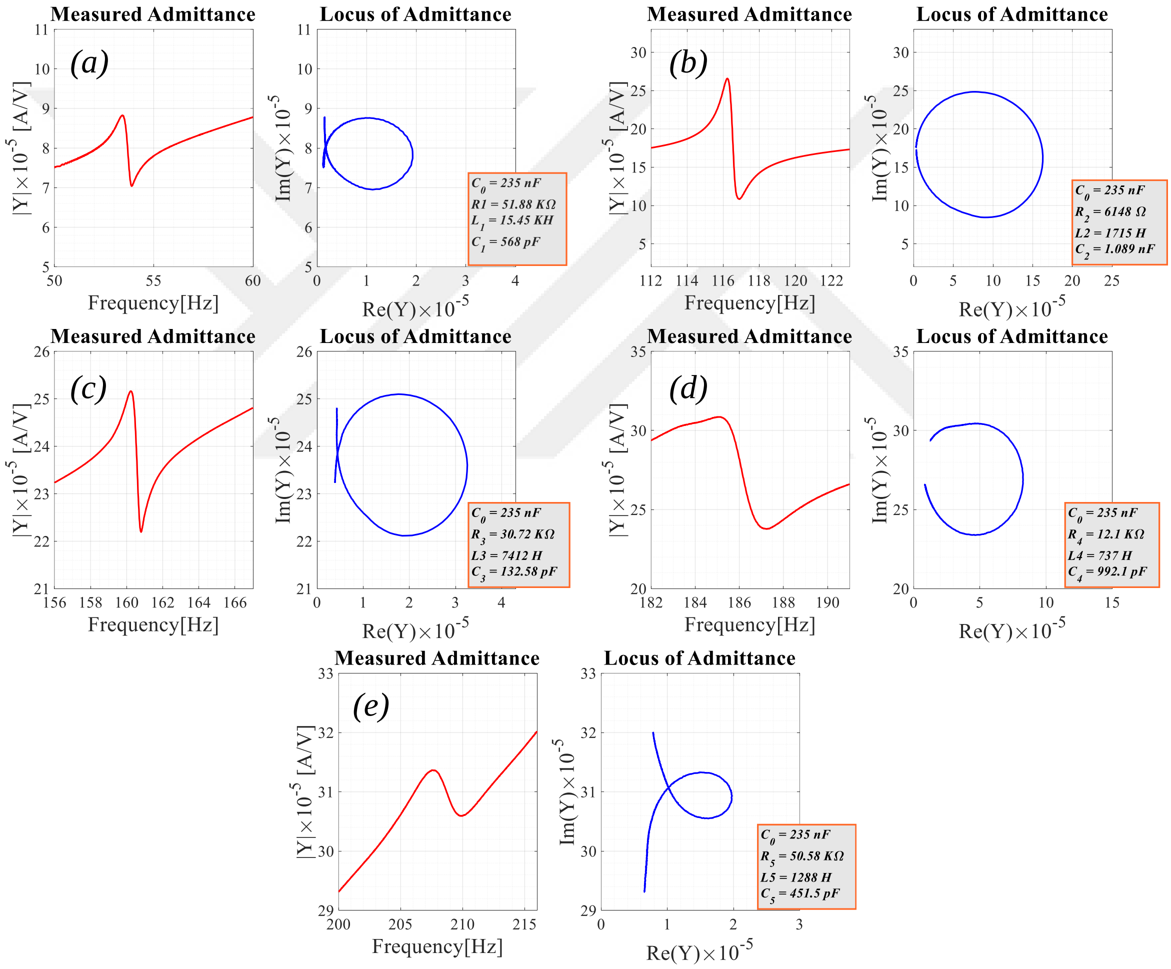

Figure 3.8: The parameters of the ECM for (a) first (b) second (c) third (d) fourth (e) fifth vibration mode identified by measuring the admittance of PZT-2. Red lines are the measured amplitude of admittance. Blue lines are the locus diagram of measured admittance.

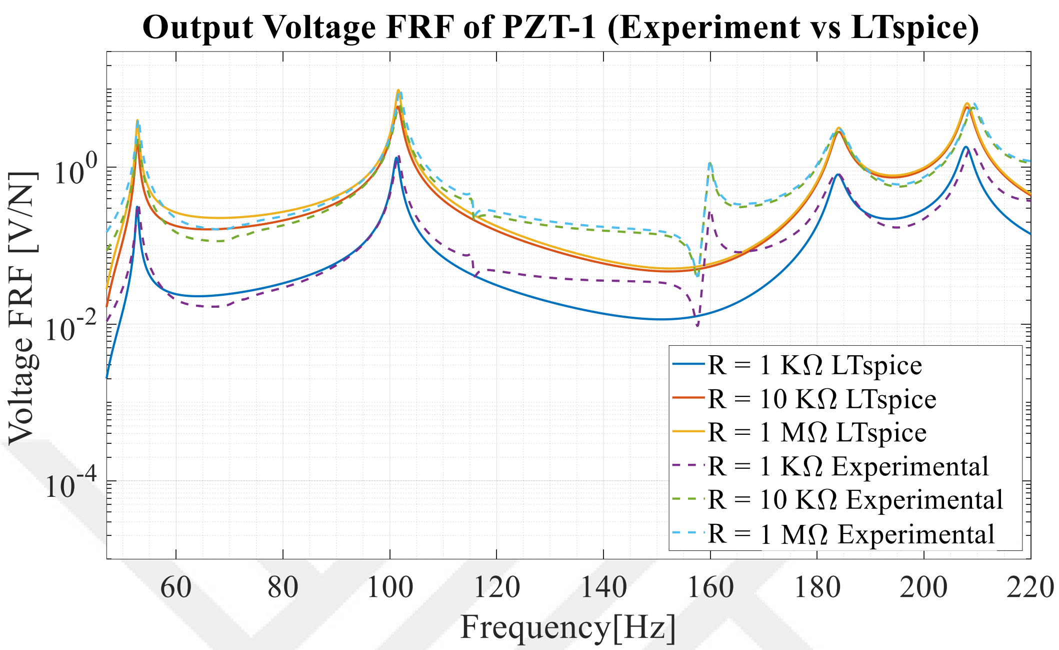

Figure 3.9: Output Voltage FRF of the PZT-1 integrated with resistive loads.

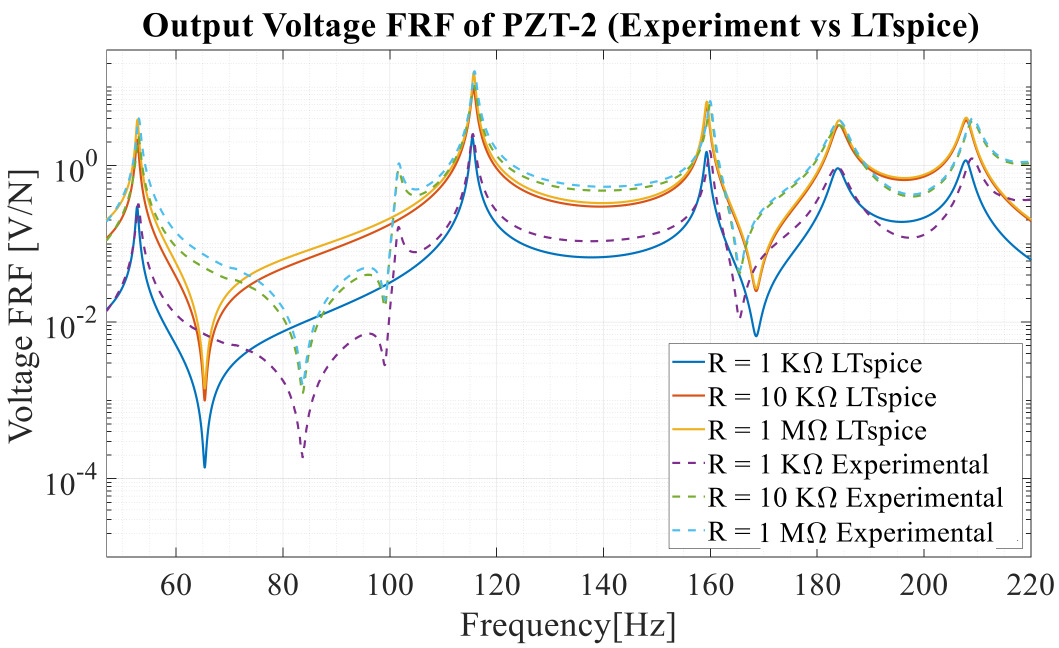

Figure 3.10: Output Voltage FRF of the PZT-2 integrated with resistive loads.

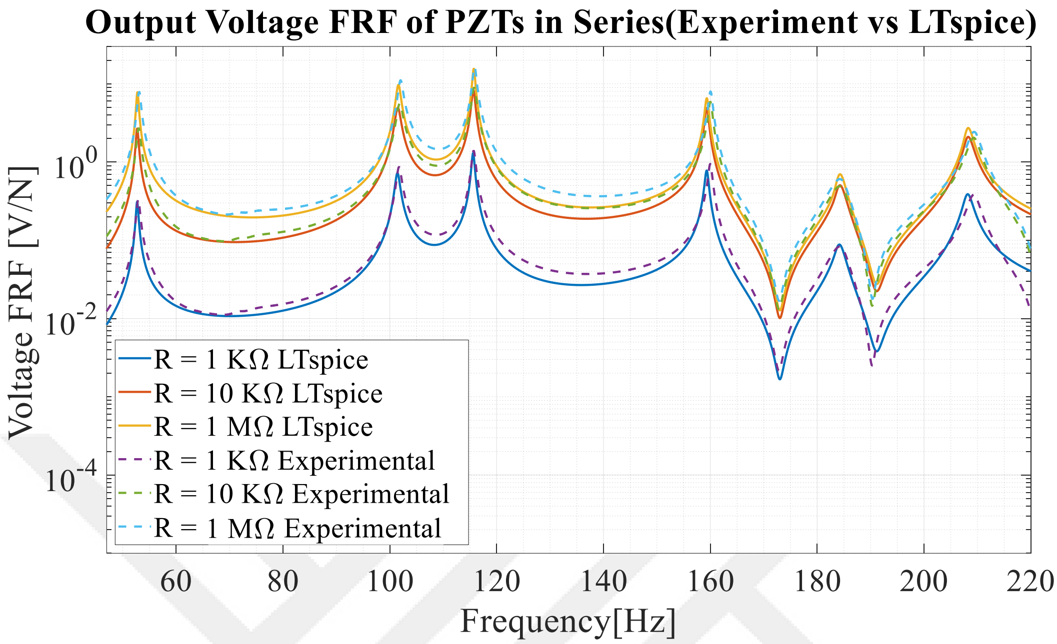

Figure 3.11: Output Voltage FRF of the MPEH in series integrated with resistive loads.

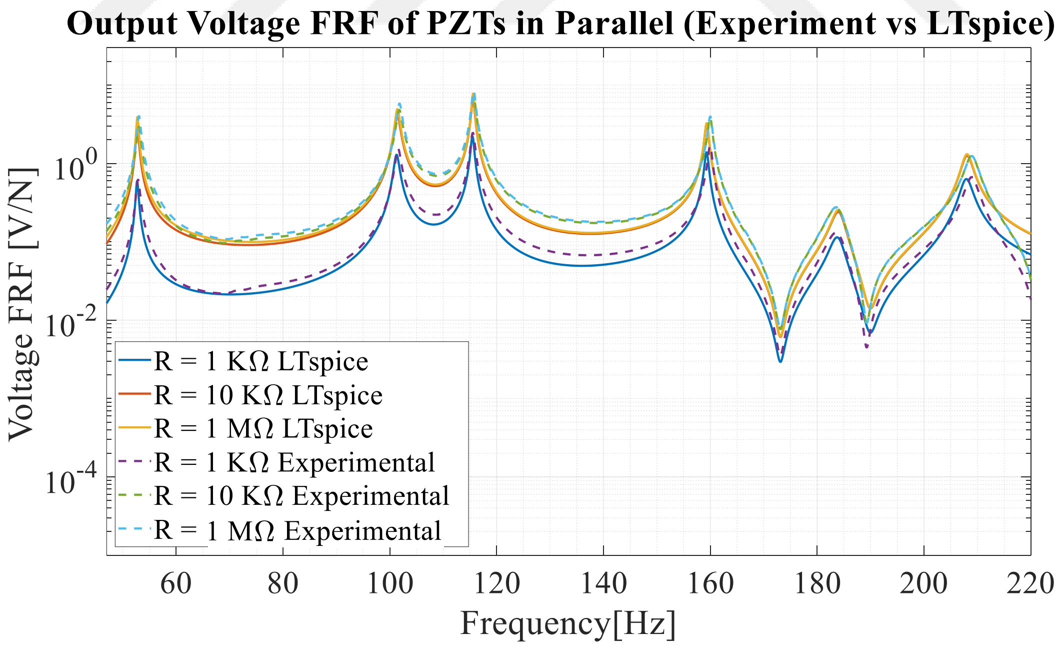

Figure 3.12: Output Voltage FRF of the MPEH in parallel integrated with resistive loads.

3.4.2 Case II: Validation with Multiple piezoelectric patches (MPEH) in series/parallel

Using multiple piezo patches on a host structure can provide a wide-band system with more efficient energy conversion. Therefore, validation of the presented methodology for multiple piezoelectric energy harvester has been carried out by connecting the PZT-1 and PZT-2 in parallel and series. Using the parameters of the ECM for PZT-1 (Figure 3.7) and PZT-2 (Figure 3.8) which has been already identified in Case I, the series and parallel configuration was developed in LTspice software. It is worth noting that the number of vibration modes of the system captured by both PZTs are the first six vibration modes of the structure in the frequency range of 0 – 230 Hz. On the other hand, the output voltage FRF of the system for series and parallel configuration has been measured experimentally and are compared with output voltage FRF obtained from the LTspice model. The results are shown in Figure 3.11 and Figure 3.12 for series and parallel configurations, respectively. The results shows that the ECM predicts the behaviour of the MPEH accurately for six vibration modes.

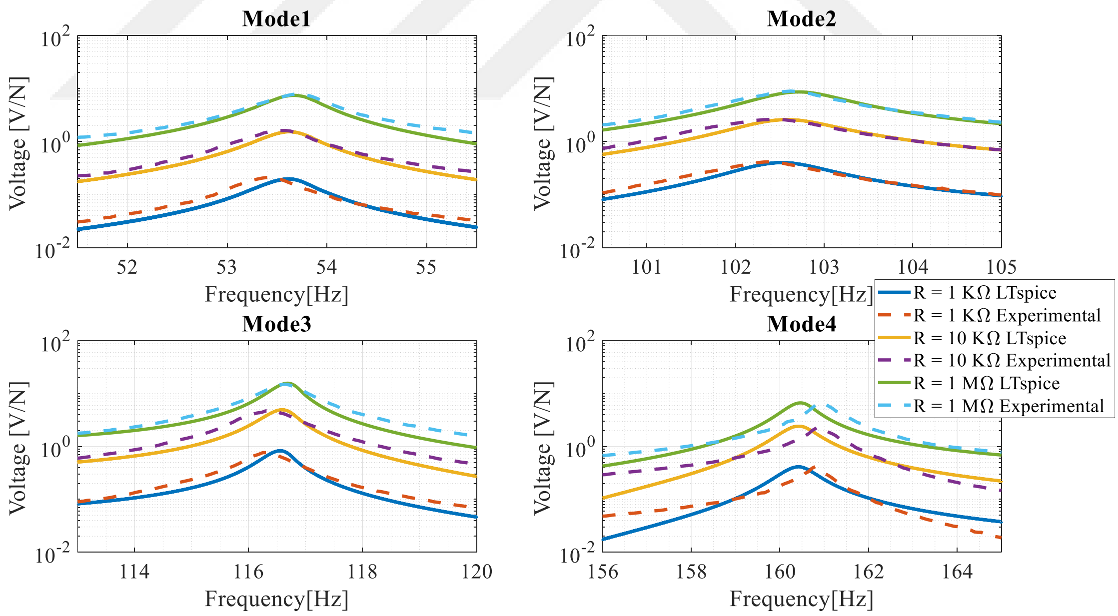

Figure 3.13: Output Voltage of the MPEH in series integrated with rectifier for three resistive loads.

3.4.3 Case III: Validation with series connected MPEH integrated with a standard rectifier

As it was mentioned before, equivalent circuit modeling is a useful tool to predict the system response when the piezoelectric energy harvester integrated with nonlinear circuit elements.

Then the system behavior can be easily simulated using circuit simulator software i.e., LTspice. The ECM of PZT-1 and PZT-2 in series configuration has been integrated with a standard rectifier in LTspice software to obtain the DC voltage output of the model around four vibration modes of the system. Besides, the DC voltage output of the actual system has been obtained by integrating a standard rectifier with the series connected PZT-1 and PZT-2. The experimental results are compared with LTspice results in Figure 3.13. It is shown that the ECM obtained with the proposed methodology can accurately predict the response of the actual setup when integrated with advanced harvesting circuits.

3.5 Discussion and Conclusion

Equivalent circuit modeling is an efficient approach to investigate piezoelectric energy harvesters with complex structural geometries integrated with advanced nonlinear harvesting circuits. A robust and accurate experimental method for identifying the multi-mode ECM directly from an experimental setup was proposed. The method is based on the electromechanical admittance of the PEH which provides information for obtaining the parameters of the ECM. The proposed experimental methodology determines the multi-mode ECM of PEH without any previous knowledge of the geometry, boundary conditions, and properties of the host structure. Besides, an experimental method was introduced to identify the equivalent voltage sources of each LCR branch of the ECM. The ECM of the harvester can be developed in LTspice software to be integrated with any harvesting circuits, either simple resistive loads or other advanced nonlinear circuits.

The validation of the method was carried out with single and multiple piezoelectric energy harvesters on a fully clamped thin plate as the host structure. Two harvesting circuits namely, resistive load and standard rectifier, were considered in the validation of the proposed methodology. At the first stage, the validation was carried out with single piezoelectric at different locations of the host structure. It was shown that the method is independent of the patch location where the multi-mode ECM of each piezo-patch, namely PZT-1 and PZT-2, can accurately predict the behavior of that patch at resonance frequencies. If the piezoelectric patch is located around the nodal points of a specific mode of the structure, it does not capture that vibration mode. Consequently, the corresponding LCR branch cannot be included in the ECM of the piezo-patch at that particular vibration mode. In this case, the corresponding vibration mode will not be observed in the admittance curve. However, since we use multiple piezo-patches at other locations, the missing modes can still be observed. It is recommended to use multiple piezo-patches on the host structure to increase the chance of observing higher number of modes. Therefore, the proposed methodology was also assessed for multiple patches on the same host structure. The ECM of PZT-1 and PZT-2 were connected in series and parallel configurations where the model has an accurate prediction of the system behavior on both resonance and off-resonance frequencies. Finally, the methodology was evaluated by series connected piezo patches integrated with a nonlinear harvesting circuit i.e., standard rectifier. It can be concluded that the proposed method is independent of the harvesting circuit and only depends on the properties of the piezoelectric patches and the host structure. This method is valid for any piezoelectric energy harvesting system with a complex host structure and the ECM can be integrated with any harvesting circuit.

CHAPTER 4
CONCLUSION, CONTRIBUTION, AND FUTURE WORKS

4.1 SSHI integrated piezoelectric energy harvesting on a plate structure

Plate-like structures, available in marine, aerospace, and automotive applications, possess close consequitive resonance frequencies, making them well-suited for broad band vibration-based piezoelectric energy harvesting. However, research on these structures for energy harvesting purposes has primarily focused on incorporating basic harvesting circuits with piezoelectric, overlooking exploration into advanced harvesting circuits. Conversely, efforts to improve the power output of piezoelectric energy harvesting through advanced harvesting circuits have been confined to simplistic mechanical models (SDOF). Therefore, Chapter 2 was dedicated to address this issue by investigating the integration of an advanced harvesting circuit i.e., synchronised switch harvesting on inductor (SSHI), with a piezoelectric patch on a fully clamped plate structure.

In Chapter 2, an analytical model was developed to predict the behavior of a piezoelectric energy harvester integrated with an SSHI circuit on a thin plate. The study involved structural analysis and employed the Rayleigh-Ritz method to obtain an electromechanical model. The equivalent impedance approach provided a closed-form solution for the system. Analytical predictions were validated experimentally, and the study explored the SSHI circuit's behavior for various force inputs and resistive loads. The experiment revealed multi-switching of the SSHI circuit at higher piezoelectric voltage levels, leading to increased energy dissipation and a significant drop in the harvester output voltage when compared with the analytical predictions. The study also compared the SSHI circuit's peak power output with a rectifier for the first two vibration modes, showing improvements at optimum resistive loads.

Studying the multiple switching behavior of the device, a coupling was observed between higher modal harmonics of the plate and the SSHI circuit's resonance at high resistive loads which results in multiple switching of the circuit at each half period of the vibration. Voltage and power output of the experimental setup subjected to several input force levels was assessed for resistive loads ranging from short circuit through open circuit and the conditions for switching behavior of the SSHI circuit was also determined.

To mitigate multiple switching behavior, it is advisable to consider the higher order harmonics of the plate-like structure as a design parameter when the SSHI circuit is developed. Ensuring that the inductor value on the switching device satisfies synchronized switching criteria and avoids multiple switching behavior is crucial when integrating SSHI circuits with plate-like structures. Exploring the addition of filters in the peak voltage detector of the switching device is another avenue worth investigating to prevent performance drops resulting from multiple switching.

The outlined bullet points summarizes the main contributions presented in Chapter 2.

- Developing an analytical model of piezoelectric energy harvester on a thin plate integrated with SSHI circuit. An analytical framework is presented by integrating the equivalent impedance of the SSHI harvesting circuit with electromechanical equations of the piezoelectric harvester on a plate.

- Acquiring a closed-form solution for mechanical vibration and electrical outputs of the system by equivalent impedance approach, and validating the electrical output predictions of the model with experimental tests.

- Comparing the performance of the SSHI with a standard rectifier for power output of the system. The improvement in the optimal power output of piezoelectric by utilizing the SSHI circuit was demonstrated, both experimentally and analytically.

- The experiment uncovered the occurrence of multi-switching in the SSHI circuit at high piezoelectric voltage levels, resulting in increased energy dissipation and a substantial decrease in the output voltage of the harvester in contrast to the anticipated values.

Chapter 2 represents the initial study in integrating advanced harvesting circuits with piezoelectric elements on plate like structures, specifically utilizing a single piezoelectric energy harvester integrated with a Parallel-SSHI circuit. Subsequent research can broaden the scope by extending the analytical model to encompass multiple piezoelectric energy harvesters on thin plate structures, exploring various connection configurations where the SSHI circuit serves as the harvesting mechanism. Furthermore, future investigations could focus on the alternative advanced harvesting circuits, such as Series-SSHI and SECE (Synchronized Electrical Charge Extraction), in conjunction with piezoelectric energy harvesters on plate structures.

4.2 Experimental approach for equivalent circuit modeling of piezoelectric energy harvesters

Various methods have been proposed for assessing the performance of energy harvesting systems. Analytical solutions have been developed to predict mechanical and electrical responses in different structures such as cantilevered beams, curved beams, M-shaped beams, and thin plates. These analytical models consider harvesting circuits as resistive loads and have been extended to include advanced harvesting circuits. The finite element method has been utilized for simulating structures with complex geometries, including M-shaped beams, L-shaped beams, and thin plates, with resistive loads as harvesting circuits. Despite the capability of analytical methods on predicting the response of harvesting systems with advanced harvesting circuits, it may lag behind in modeling systems with complex geometries. On the other hand, commercial finite element softwares pave the way for modeling harvesting systems with complex geometries in the host structure; however, they are not capable of simulating advanced harvesting circuits. An alternative method has been proposed which approximates the piezoelectric energy harvester by an equivalent circuit model. Then the equivalent circuit model can be simulated in a circuit simulator software like LTSpice and be investigated with any desired harvesting circuit including advanced harvesting circuits with nonlinear electrical circuit components such as SSHI circuits as discussed in the previous chapter.

Equivalent circuit modeling (ECM) for piezoelectric energy harvesters proves to be advantageous particularly for host structures with complex geometries and when the system is integrated with advanced harvesting circuits. Previously, analytical and finite element models have been used to identify the equivalent circuit model of the piezoelectric energy harvesters. Yet, those methods require accurate analytical and/or numerical representation of the piezoelectric energy harvesters. Therefore, Chapter 3 focused on overcoming the limitations of previous analytical and finite element methods by presenting an innovative experimental admittance-based system identification technique. This approach allows the calculation of the multi-modal Equivalent Circuit Modeling (ECM) without prior knowledge of the host structur's geometry and/or the physical properties of the piezoelectric patches.

The main contributions of Chapter 3 is highlighted as follows:

- Presenting a robust and accurate experimental system identification method based on electromechanical admittance measurement of piezoelectric energy harvester to determine the multi-modal equivalent circuit model of the system.
- Introducing an experimental method to identify the equivalent voltage sources which correspond to the contribution of input point force in modal cordinates.
- Validating the proposed methodology for several case studies i.e., single and multiple piezoelectric energy harvesters integrated with a resistive load and a standard rectifier.

It was shown that the method is independent of the patch location where the multi-mode ECM of each piezo-patch, namely PZT-1 and PZT-2, can accurately predict the behavior of that patch at vibration modes observed by the corresponding patch. The proposed method predicts the properties of the system independent of the harvesting circuit and only depends on the properties of the piezoelectric patches and the host structure. This method is valid for extracting the ECM of any piezoelectric energy harvesting system with a complex host structure, structurally coupled with a single and/or multiple piezo-patches. Then the ECM can be integrated with any harvesting circuit i.e, linear or nonlinear circuit.

The proposed methodology is beneficial when there is no physical model such as analytical or FE models. It provides information of the system in modal coordinates using the measured admittance of the system. While this methodology does not provide direct information about the physical model, it can be used together with other experimental measurements to enhance the overall understanding of the system properties. In future research, the scope of this methodology could be broadened to establish an experimental framework for retrieving the physical model of the system. Subsequently, this model could facilitate the development of an efficient system, enabling the prediction of optimal placements for piezoelectric patches on the structure.

BIBLIOGRAPHY

[Aghakhani & Basdogan, 2017] Aghakhani, A., & Basdogan, I. (2017). Equivalent Impedance Electroelastic Modeling of Multiple Piezo-Patch Energy Harvesters on a Thin Plate With AC–DC Conversion. *IEEE/ASME Transactions on Mechatronics*, *22*(4), 1575-1584. https://doi.org/10.1109/TMECH.2017.2712713

[Aghakhani & Basdogan, 2018] Aghakhani, A., & Basdogan, I. (2018). *Multiple piezo-patch energy harvesters on a thin plate with respective AC-DC conversion* (Vol. 10595). SPIE. https://doi.org/10.1117/12.2296831

[Ahmad et al., 2016] Ahmad, M. R., Khan, M. R. A. A., & Rahman, M. A. (2016). Energy harvesting based on cantilever beam for different piezoelectric materials from acoustic vibration by simulation process. 2016 9th International Conference on Electrical and Computer Engineering (ICECE),

[Aridogan et al., 2013] Aridogan, U., Basdogan, I., & Erturk, A. (2013). Electroelastic Finite Element Modeling and Experimental Validation of Structurally-Integrated Piezoelectric Energy Harvester. International Design Engineering Technical Conferences and Computers and Information in Engineering Conference,

[Aridogan et al., 2014] Aridogan, U., Basdogan, I., & Erturk, A. (2014). Analytical modeling and experimental validation of a structurally integrated piezoelectric energy harvester on a thin plate. *Smart Materials and Structures*, *23*(4), 045039.

[Aridogan et al., 2014] Aridogan, U., Basdogan, I., & Erturk, A. (2014). Multiple patch–based broadband piezoelectric energy harvesting on plate-based structures. *Journal of Intelligent Material Systems and Structures*, *25*(14), 1664-1680.

[Bayik et al., 2016] Bayik, B., Aghakhani, A., Basdogan, I., & Erturk, A. (2016). Equivalent circuit modeling of a piezo-patch energy harvester on a thin plate with AC–DC conversion. *Smart Materials and Structures*, *25*(5), 055015. https://doi.org/10.1088/0964-1726/25/5/055015

[Ben Ayed et al., 2013] Ben Ayed, S., Abdelkefi, A., Najar, F., & Hajj, M. R. (2013). Design and performance of variable-shaped piezoelectric energy harvesters. *Journal of*

Intelligent Material Systems and Structures, *25*(2), 174-186. https://doi.org/10.1177/1045389X13489365

[Cai et al., 2021] Cai, Y., Zhang, K., Ye, Z., Liu, C., Lu, K., & Wang, L. (2021). Influence of Temperature on the Natural Vibration Characteristics of Simply Supported Reinforced Concrete Beam. *Sensors (Basel)*, *21*(12). https://doi.org/10.3390/s21124242

[Chen et al., 2021] Chen, K., Gao, F., Liu, Z., & Liao, W.-H. (2021). A nonlinear M-shaped tri-directional piezoelectric energy harvester. *Smart Materials and Structures*, *30*(4), 045017. https://doi.org/10.1088/1361-665X/abe87e

[Chen et al., 2020] Chen, Z., Xia, Y., He, J., Xiong, Y., & Wang, G. (2020). Elastic-electro-mechanical modeling and analysis of piezoelectric metamaterial plate with a self-powered synchronized charge extraction circuit for vibration energy harvesting. *Mechanical Systems and Signal Processing*, *143*, 106824. https://doi.org/https://doi.org/10.1016/j.ymssp.2020.106824

[Claude Richard, 2007] Claude Richard, D. G., Elie Lefeuvre (2007). *Self-powered electronic breaker with automatic switching by detecting maxima or minima of potential difference between its power electrodes*.

[Cottone et al., 2012] Cottone, F., Gammaitoni, L., Vocca, H., Ferrari, M., & Ferrari, V. (2012). Piezoelectric buckled beams for random vibration energy harvesting. *Smart Materials and Structures*, *21*(3), 035021.

[Dietl & Garcia, 2010] Dietl, J. M., & Garcia, E. (2010). Beam Shape Optimization for Power Harvesting. *Journal of Intelligent Material Systems and Structures*, *21*(6), 633-646. https://doi.org/10.1177/1045389X10365094

[Eltamaly & Addoweesh, 2017] Eltamaly, A. M., & Addoweesh, K. E. (2017). A Novel Self-Power SSHI Circuit for Piezoelectric Energy Harvester. *IEEE Transactions on Power Electronics*, *32*(10), 7663-7673. https://doi.org/10.1109/tpel.2016.2636903

[Elvin & Elvin, 2008] Elvin, N. G., & Elvin, A. A. (2008). A General Equivalent Circuit Model for Piezoelectric Generators. *Journal of Intelligent Material Systems and Structures*, *20*(1), 3-9. https://doi.org/10.1177/1045389X08089957

[Erturk, 2012] Erturk, A. (2012). Assumed-modes modeling of piezoelectric energy harvesters: Euler–Bernoulli, Rayleigh, and Timoshenko models with axial deformations. *Computers & Structures*, *106-107*, 214-227. https://doi.org/https://doi.org/10.1016/j.compstruc.2012.05.010

[Erturk & Inman, 2008a] Erturk, A., & Inman, D. J. (2008a). A Distributed Parameter Electromechanical Model for Cantilevered Piezoelectric Energy Harvesters. *Journal of Vibration and Acoustics*, *130*(4). https://doi.org/10.1115/1.2890402

[Erturk & Inman, 2008b] Erturk, A., & Inman, D. J. (2008b). Issues in mathematical modeling of piezoelectric energy harvesters. *Smart Materials and Structures*, *17*(6), 065016. https://doi.org/10.1088/0964-1726/17/6/065016

[Erturk & Inman, 2009] Erturk, A., & Inman, D. J. (2009). An experimentally validated bimorph cantilever model for piezoelectric energy harvesting from base excitations. *Smart Materials and Structures*, *18*(2), 025009.

[Erturk et al., 2009] Erturk, A., Renno, J. M., & Inman, D. J. (2009). Modeling of Piezoelectric Energy Harvesting from an L-shaped Beam-mass Structure with an Application to UAVs. *Journal of Intelligent Material Systems and Structures*, *20*(5), 529-544. https://doi.org/10.1177/1045389x08098096

[Guan & Liao, 2009] Guan, M. J., & Liao, W. H. (2009). On the Equivalent Circuit Models of Piezoelectric Ceramics. *Ferroelectrics*, *386*(1), 77-87. https://doi.org/10.1080/00150190902961439

[Guyomar et al., 2005a] Guyomar, D., Badel, A., Lefeuvre, E., & Richard, C. (2005a). Toward energy harvesting using active materials and conversion improvement by nonlinear processing. *IEEE Transactions on Ultrasonics, Ferroelectrics and Frequency Control*, *52*(4), 584-595. https://doi.org/10.1109/tuffc.2005.1428041

[Guyomar et al., 2005b] Guyomar, D., Badel, A., Lefeuvre, E., & Richard, C. (2005b). Toward energy harvesting using active materials and conversion improvement by nonlinear processing. *IEEE Transactions on Ultrasonics, Ferroelectrics, and Frequency Control*, *52*(4), 584-595. https://doi.org/10.1109/TUFFC.2005.1428041

[Hagmann, 2019] Hagmann, M. (2019). Analysis and equivalent circuit for accurate wideband calculations of the impedance for a piezoelectric transducer having loss. *AIP Advances*, *9*(8), 085313.

[Hoseyni et al., 2023] Hoseyni, S. M., Simsek, M., Aghakhani, A., Lefeuvre, E., & Basdogan, I. (2023). Multimodal piezoelectric energy harvesting on a thin plate integrated with SSHI circuit: an analytical and experimental study. *Smart Materials and Structures*, *32*(9), 095024. https://doi.org/10.1088/1361-665X/ace9a0

[Huang et al., 2020] Huang, H., Xu, Z., Wang, J., & Dong, J. (2020). A low frequency operation high speed stick-slip piezoelectric actuator achieved by using a L-shape flexure hinge. *Smart Materials and Structures*, *29*(6), 065007. https://doi.org/10.1088/1361-665X/ab8315

[Ikeda, 1990] Ikeda, T. (1990). *Fundamentals of Piezoelectricity*. Oxford University Press. https://books.google.com.tr/books?id=FW14QgAACAAJ

[Jung et al., 2015] Jung, W.-S., Lee, M.-J., Kang, M.-G., Moon, H. G., Yoon, S.-J., Baek, S.-

H., & Kang, C.-Y. (2015). Powerful curved piezoelectric generator for wearable applications. *Nano Energy*, *13*, 174-181. https://doi.org/https://doi.org/10.1016/j.nanoen.2015.01.051

[Jung et al., 2016] Jung, W.-S., Lee, M., Baek, S.-H., Jung, I. K., Yoon, S.-J., & Kang, C.-Y. (2016). Structural approaches for enhancing output power of piezoelectric polyvinylidene fluoride generator. *Nano Energy*, *22*, 514-523. https://doi.org/https://doi.org/10.1016/j.nanoen.2016.02.043

[Junrui & Wei-Hsin, 2010] Junrui, L., & Wei-Hsin, L. (2010). Impedance matching for improving piezoelectric energy harvesting systems. Proc.SPIE,

[Lallart et al., 2008] Lallart, M., Lefeuvre, É., Richard, C., & Guyomar, D. (2008). Self-powered circuit for broadband, multimodal piezoelectric vibration control. *Sensors and Actuators A: Physical*, *143*(2), 377-382. https://doi.org/https://doi.org/10.1016/j.sna.2007.11.017

[Lallart et al., 2011] Lallart, M., Wu, Y.-C., & Guyomar, D. (2011). Switching delay effects on nonlinear piezoelectric energy harvesting techniques. *IEEE Transactions on Industrial Electronics*, *59*(1), 464-472.

[Lan et al., 2022] Lan, C., Liao, Y., & Hu, G. (2022). A unified equivalent circuit and impedance analysis method for galloping piezoelectric energy harvesters. *Mechanical Systems and Signal Processing*, *165*, 108339. https://doi.org/https://doi.org/10.1016/j.ymssp.2021.108339

[Leadenham & Erturk, 2015] Leadenham, S., & Erturk, A. (2015). Nonlinear M-shaped broadband piezoelectric energy harvester for very low base accelerations: primary and secondary resonances. *Smart Materials and Structures*, *24*(5), 055021. https://doi.org/10.1088/0964-1726/24/5/055021

[Lefeuvre et al., 2006] Lefeuvre, E., Badel, A., Richard, C., Petit, L., & Guyomar, D. (2006). A comparison between several vibration-powered piezoelectric generators for standalone systems. *Sensors and Actuators A: Physical*, *126*(2), 405-416.

[Leinonen et al., 2013] Leinonen, M., Palosaari, J., Juuti, J., & Jantunen, H. (2013). Combined electrical and electromechanical simulations of a piezoelectric cymbal harvester for energy harvesting from walking. *Journal of Intelligent Material Systems and Structures*, *25*(4), 391-400. https://doi.org/10.1177/1045389X13500573

[Li & Lee, 2022] Li, T., & Lee, P. S. (2022). Piezoelectric Energy Harvesting Technology: From Materials, Structures, to Applications. *Small Structures*, *3*(3), 2100128. https://doi.org/https://doi.org/10.1002/sstr.202100128

[Liang & Liao, 2011] Liang, J., & Liao, W.-H. (2011). Energy flow in piezoelectric energy harvesting systems. *Smart Materials and Structures*, *20*(1), 015005. https://doi.org/10.1088/0964-1726/20/1/015005

[Liang & Liao, 2012a] Liang, J., & Liao, W. H. (2012a). Impedance Modeling and Analysis for Piezoelectric Energy Harvesting Systems. *IEEE/ASME Transactions on Mechatronics*, *17*(6), 1145-1157. https://doi.org/10.1109/TMECH.2011.2160275

[Liang & Liao, 2012b] Liang, J., & Liao, W. H. (2012b). Improved Design and Analysis of Self-Powered Synchronized Switch Interface Circuit for Piezoelectric Energy Harvesting Systems. *IEEE Transactions on Industrial Electronics*, *59*(4), 1950-1960. https://doi.org/10.1109/TIE.2011.2167116

[Liang & Liao, 2008] Liang, J. R., & Liao, W. H. (2008). Piezoelectric Energy Harvesting and Dissipation on Structural Damping. *Journal of Intelligent Material Systems and Structures*, *20*(5), 515-527. https://doi.org/10.1177/1045389X08098194

[Liang & Liao, 2011] Liang, J. R., & Liao, W. H. (2011). On the Influence of Transducer Internal Loss in Piezoelectric Energy Harvesting with SSHI Interface. *Journal of Intelligent Material Systems and Structures*, *22*(5), 503-512. https://doi.org/10.1177/1045389X11401447

[Liao & Liang, 2018] Liao, Y., & Liang, J. (2018). Maximum power, optimal load, and impedance analysis of piezoelectric vibration energy harvesters. *Smart Materials and Structures*, *27*(7), 075053. https://doi.org/10.1088/1361-665X/aaca56

[Liao & Liang, 2019] Liao, Y., & Liang, J. (2019). Unified modeling, analysis and comparison of piezoelectric vibration energy harvesters. *Mechanical Systems and Signal Processing*, *123*, 403-425. https://doi.org/https://doi.org/10.1016/j.ymssp.2019.01.025

[Lien & Shu, 2012] Lien, I., & Shu, Y. (2012). Array of piezoelectric energy harvesting by the equivalent impedance approach. *Smart Materials and Structures*, *21*(8), 082001.

[Lien et al., 2010] Lien, I., Shu, Y., Wu, W., Shiu, S., & Lin, H. (2010). Revisit of series-SSHI with comparisons to other interfacing circuits in piezoelectric energy harvesting. *Smart Materials and Structures*, *19*(12), 125009.

[Lien et al., 2010] Lien, I. C., Shu, Y. C., Wu, W. J., Shiu, S. M., & Lin, H. C. (2010). Revisit of series-SSHI with comparisons to other interfacing circuits in piezoelectric energy harvesting. *Smart Materials and Structures*, *19*(12), 125009. https://doi.org/10.1088/0964-1726/19/12/125009

[Lin et al., 2013] Lin, H. C., Wu, P. H., Lien, I. C., & Shu, Y. C. (2013). Analysis of an array of piezoelectric energy harvesters connected in series. *Smart Materials and Structures*, *22*(9), 094026. https://doi.org/10.1088/0964-1726/22/9/094026

[Ottman et al., 2002] Ottman, G. K., Hofmann, H. F., Bhatt, A. C., & Lesieutre, G. A. (2002).

Adaptive piezoelectric energy harvesting circuit for wireless remote power supply. *IEEE Transactions on Power Electronics*, *17*(5), 669-676. https://doi.org/10.1109/tpel.2002.802194

[Priya & Inman, 2008] Priya, S., & Inman, D. J. (2008). *Energy Harvesting Technologies*. Springer US. https://books.google.com.tr/books?id=Ch74D9Y3t2AC

[Qian et al., 2021] Qian, F., Liao, Y., Zuo, L., & Jones, P. (2021). System-level finite element analysis of piezoelectric energy harvesters with rectified interface circuits and experimental validation. *Mechanical Systems and Signal Processing*, *151*, 107440. https://doi.org/https://doi.org/10.1016/j.ymssp.2020.107440

[Raju et al., 2017] Raju, S. S., Umapathy, M., & Uma, G. (2017). High-output piezoelectric energy harvester using tapered beam with cavity. *Journal of Intelligent Material Systems and Structures*, *29*(5), 800-815. https://doi.org/10.1177/1045389X17721044

[Salmani & Rahimi, 2018] Salmani, H., & Rahimi, G. H. (2018). Study the Effect of Tapering on the Nonlinear Behavior of an Exponentially Varying Width Piezoelectric Energy Harvester. *Journal of Vibration and Acoustics*, *140*(6). https://doi.org/10.1115/1.4039932

[Seok et al., 2022] Seok, S., Brenes, A., Yoo, C., & Lefeuvre, E. (2022). Experiment and analysis of a piezoelectric energy harvester based on combined FEM modeling and spice simulation. *Microsystem Technologies*, *28*(9), 2123-2130. https://doi.org/10.1007/s00542-022-05355-z

[Sezer & Koç, 2021] Sezer, N., & Koç, M. (2021). A comprehensive review on the state-of-the-art of piezoelectric energy harvesting. *Nano Energy*, *80*, 105567. https://doi.org/https://doi.org/10.1016/j.nanoen.2020.105567

[Sharma et al., 2022] Sharma, S., Kiran, R., Azad, P., & Vaish, R. (2022). A review of piezoelectric energy harvesting tiles: Available designs and future perspective. *Energy Conversion and Management*, *254*, 115272. https://doi.org/10.1016/j.enconman.2022.115272

[Shu & Lien, 2006] Shu, Y., & Lien, I. (2006). Analysis of power output for piezoelectric energy harvesting systems. *Smart Materials and Structures*, *15*(6), 1499.

[Shu et al., 2007] Shu, Y., Lien, I., & Wu, W. (2007). An improved analysis of the SSHI interface in piezoelectric energy harvesting. *Smart Materials and Structures*, *16*(6), 2253.

[Shu & Lien, 2006] Shu, Y. C., & Lien, I. C. (2006). Analysis of power output for piezoelectric energy harvesting systems. *Smart Materials and Structures*, *15*(6), 1499. https://doi.org/10.1088/0964-1726/15/6/001

[Shu et al., 2007] Shu, Y. C., Lien, I. C., & Wu, W. J. (2007). An improved analysis of the SSHI interface in piezoelectric energy harvesting. *Smart Materials and Structures*, *16*(6), 2253. https://doi.org/10.1088/0964-1726/16/6/028

[Sobral & Santos, 2013] Sobral, T. C., & Santos, E. J. (2013). Parameter extraction methods for piezoelectric-based transducer design. 28th Symposium on Microelectronics Technology and Devices (SBMicro 2013),

[Syed et al., 2018] Syed, W. U., Bojesomo, A., & Elfadel, I. M. (2018). Electromechanical Model of a Tapered Piezoelectric Energy Harvester. *IEEE Sensors Journal*, *18*(14), 5853-5862. https://doi.org/10.1109/JSEN.2018.2841359

[Tang et al., 2010] Tang, L., Yang, Y., & Soh, C. K. (2010). Toward Broadband Vibration-based Energy Harvesting. *Journal of Intelligent Material Systems and Structures*, *21*(18), 1867-1897. https://doi.org/10.1177/1045389x10390249

[Tian et al., 2020] Tian, W., Shi, Y., Cui, H., & Shi, J. (2020). Research on piezoelectric energy harvester based on coupled oscillator model for vehicle vibration utilizing a L-shaped cantilever beam. *Smart Materials and Structures*, *29*(7), 075014. https://doi.org/10.1088/1361-665X/ab87e1

[Wang et al., 2020] Wang, B., Li, Z., & Yang, Z. (2020). A distributed-parameter electromechanical coupling model for a piezoelectric energy harvester with variable curvature. *Smart Materials and Structures*, *29*(11), 115015. https://doi.org/10.1088/1361-665X/abad4e

[Wang et al., 2022] Wang, P.-H., Liu, H.-T., & Wang, Y.-B. (2022). Electromechanical behavior of 3-3 piezoelectric star-shaped metamaterial with four types of connection. *Mechanical Systems and Signal Processing*, *170*, 108825. https://doi.org/https://doi.org/10.1016/j.ymssp.2022.108825

[Wu et al., 2021] Wu, N., Bao, B., & Wang, Q. (2021). Review on engineering structural designs for efficient piezoelectric energy harvesting to obtain high power output. *Engineering Structures*, *235*, 112068. https://doi.org/https://doi.org/10.1016/j.engstruct.2021.112068

[Xie et al., 2020] Xie, X., Wang, Z., Liu, D., Du, G., & Zhang, J. (2020). An experimental study on a novel cylinder harvester made of L-shaped piezoelectric coupled beams with a high efficiency. *Energy*, *212*, 118752. https://doi.org/10.1016/j.energy.2020.118752

[Xie et al., 2017] Xie, X. D., Carpinteri, A., & Wang, Q. (2017). A theoretical model for a piezoelectric energy harvester with a tapered shape. *Engineering Structures*, *144*, 19-25. https://doi.org/https://doi.org/10.1016/j.engstruct.2017.04.050

[Yang & Tang, 2009] Yang, Y., & Tang, L. (2009). Equivalent Circuit Modeling of Piezoelectric Energy Harvesters. *Journal of Intelligent Material Systems and Structures*, *20*(18), 2223-2235. https://doi.org/10.1177/1045389X09351757

[Yang et al., 2017] Yang, Z., Erturk, A., & Zu, J. (2017). On the efficiency of piezoelectric energy harvesters. *Extreme Mechanics Letters*, *15*, 26-37. https://doi.org/https://doi.org/10.1016/j.eml.2017.05.002

[Yoon et al., 2016] Yoon, H., Youn, B. D., & Kim, H. S. (2016). Kirchhoff plate theory-based electromechanically-coupled analytical model considering inertia and stiffness effects of a surface-bonded piezoelectric patch. *Smart Materials and Structures*, *25*(2), 025017.

[Zhang et al., 2021] Zhang, Z., Xiang, H., & Tang, L. (2021). Modeling, analysis and comparison of four charging interface circuits for piezoelectric energy harvesting. *Mechanical Systems and Signal Processing*, *152*, 107476. https://doi.org/https://doi.org/10.1016/j.ymssp.2020.107476

[Zheng et al., 2015] Zheng, X., Zhang, Z., Zhu, Y., Mei, J., Peng, S., Li, L., & Yu, Y. (2015). Analysis of Energy Harvesting Performance for d_{15} Mode Piezoelectric Bimorph in Series Connection Based on Timoshenko Beam Model. *IEEE/ASME Transactions on Mechatronics*, *20*(2), 728-739. https://doi.org/10.1109/tmech.2014.2316520

[Zhou et al., 2016] Zhou, S., Cao, J., Inman, D. J., Lin, J., & Li, D. (2016). Harmonic balance analysis of nonlinear tristable energy harvesters for performance enhancement. *Journal of Sound and Vibration*, *373*, 223-235. https://doi.org/https://doi.org/10.1016/j.jsv.2016.03.017

[Zhou et al., 2021] Zhou, W., Wang, B., Lim, C. W., & Yang, Z. (2021). A distributed-parameter electromechanical coupling model for a segmented arc-shaped piezoelectric energy harvester. *Mechanical Systems and Signal Processing*, *146*, 107005. https://doi.org/https://doi.org/10.1016/j.ymssp.2020.107005